3

Prime Movers

3.1 Introduction 3-1
3.2 Steam Turbines 3-3
3.3 Steam Turbine Modeling 3-5
3.4 Speed Governors for Steam Turbines 3-10
3.5 Gas Turbines 3-11
3.6 Diesel Engines 3-12
Diesel-Engine Operation • Diesel-Engine Modeling
3.7 Stirling Engines 3-17
Summary of Thermodynamic Basic Cycles • The Stirling-Cycle Engine • Free-Piston Stirling Engines Modeling
3.8 Hydraulic Turbines 3-24
Hydraulic Turbines Basics • A First-Order Ideal Model of Hydraulic Turbines • Second- and Higher-Order Models of Hydraulic Turbines • Hydraulic Turbine Governors • Reversible Hydraulic Machines
3.9 Wind Turbines 3-39
Principles and Efficiency of Wind Turbines • The Steady-State Model of Wind Turbines • Wind Turbine Models for Control
3.10 Summary 3-52
References 3-54

3.1 Introduction

Electric generators convert mechanical energy into electrical energy. The mechanical energy is produced by prime movers. Prime movers are mechanical machines. They convert primary energy of a fuel or fluid into mechanical energy. They are also called turbines or engines. The fossil fuels commonly used in prime movers are coal, gas, oil, or nuclear fuel.

Essentially, the fossil fuel is burned in a combustor; thus, thermal energy is produced. Thermal energy is then taken by a working fluid and turned into mechanical energy in the prime mover.

Steam is the working fluid for coal or nuclear fuel turbines. In gas turbines or in diesel or internal combustion engines, the working fluid is the gas or oil in combination with air.

On the other hand, the potential energy of water from an upper-level reservoir may be turned into kinetic energy that hits the runner of a hydraulic turbine, changes momentum and direction, and produces mechanical work at the turbine shaft as it rotates against the "braking" torque of the electric generator under electric load.

Wave energy is similarly converted into mechanical work in special tidal hydraulic turbines. Wind kinetic energy is converted by wind turbines into mechanical energy.

A complete classification of prime movers is difficult due to the many variations in construction, from topology to control. However, a simplified prime mover classification is described in Table 3.1.

TABLE 3.1 Prime Mover Classification

Fuel	Working Fluid	Power Range	Main Applications	Type	Observation
Coal or nuclear fuel	Steam	Up to 1500 MW/unit	Electric power systems	Steam turbines	High speed
Gas or oil	Gas (oil) + air	From watts to hundreds of MW/unit	Large and distributed power systems, automotive applications (vessels, trains, highway and off-highway vehicles), autonomous power sources	Gas turbines, diesel engines, internal combustion engines, Stirling engines	With rotary but also linear reciprocating motion
Water energy	Water	Up to 1000 MW/unit	Large and distributed electric power systems, autonomous power sources	Hydraulic turbines	Medium and low speeds, >75 rpm
Wind energy	Air	Up to 5 MW/unit	Distributed power systems, autonomous power sources	Wind or wave turbines	Speed down to 10 rpm

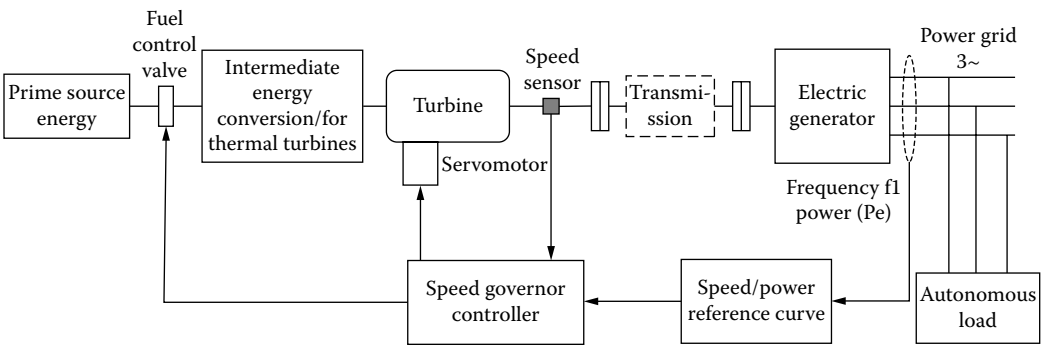

FIGURE 3.1 Basic prime-mover generator system.

In general, a prime mover or turbine drives an electric generator directly, or through a transmission (at power less than a few megawatts [MW]), Figure 3.1, [1–3]. The prime mover is necessarily provided with a so-called speed governor (in fact, a speed control and protection system) that properly regulates the speed, according to electric generator frequency/power curves (Figure 3.2).

Notice that the turbine is provided with a servomotor that activates one or a few control valves that regulate the fuel (or fluid) flow in the turbine, thus controlling the mechanical power at the turbine shaft. The speed at the turbine shaft is measured precisely and compared with the reference speed. The speed controller then acts on the servomotor to open or close control valves and control speed as required. The reference speed is not constant. In alternating current (AC) power systems, with generators in parallel, a speed drop of 2 to 3% is allowed, with power increased to the rated value [1–3].

The speed drop is required for two reasons:

- With a few generators of different powers in parallel, fair (proportional) power load sharing is provided.
- When power increases too much, the speed decreases accordingly, signaling that the turbine has to be shut off.

In Figure 3.2, at point A at the intersection between generator power and turbine power, speed is statically stable, as any departure from this point would provide the conditions (through motion equation) to return to it.

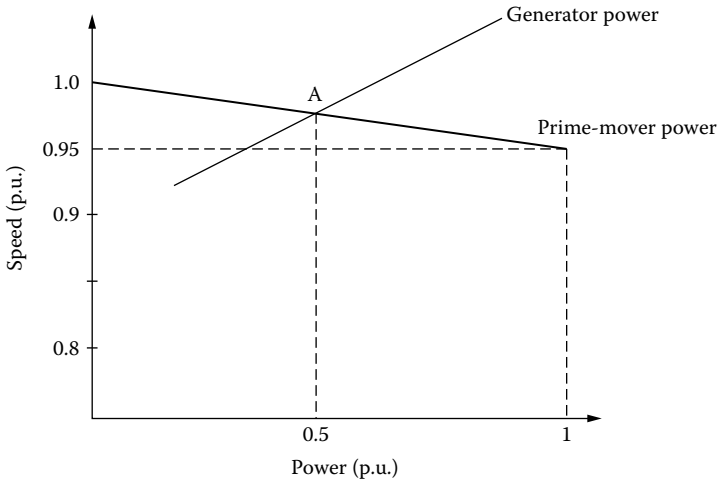

FIGURE 3.2 The reference speed (frequency)/power curve.

With synchronous generators operating in a constant voltage and frequency power system, the speed drop is very small, which implies strong strains on the speed governor due to inertia and so forth. It also leads to slower power control. On the other hand, the use of doubly fed induction generators, or of AC generators with full power electronics between them and the power system, would allow for speed variation (and control) in larger ranges (±20% and more). That is, a smaller speed reference for lower power. Power sharing between electric generators would then be done through power electronics in a much faster and more controlled manner. Once these general aspects of prime mover requirements are clarified, we will deal in some detail with prime movers in terms of principles, steady-state performance, and models for transients. The main speed governors and their dynamic models are also included for each main type of prime mover investigated here.

3.2 Steam Turbines

Coal, oil, and nuclear fuels are burned to produce high pressure, high temperature, and steam in a boiler. The potential energy in the steam is then converted into mechanical energy in the so-called axial-flow steam turbines.

The steam turbines contain stationary and rotating blades grouped into stages: high pressure (HP), intermediate pressure (IP), low pressure (LP), and so forth. The high-pressure steam in the boiler is let to enter — through the main emergency stop valves (MSVs) and the governor valves (GVs) — the stationary blades, where it is accelerated as it expands to a lower pressure (Figure 3.3). Then the fluid is guided into the rotating blades of the steam turbine, where it changes momentum and direction, thus exerting a tangential force on the turbine rotor blades. Torque on the shaft and, thus, mechanical power, are produced. The pressure along the turbine stages decreases, and thus, the volume increases. Consequently, the length of the blades is lower in the high-pressure stages than in the lower-power stages.

The two, three, or more stages (HP, IP, and LP) are all, in general, on the same shaft, working in tandem. Between stages, the steam is reheated, its enthalpy is increased, and the overall efficiency is improved — up to 45% for modern coal-burn steam turbines.

Nonreheat steam turbines are built below 100 MW, while single-reheat and double-reheat steam turbines are common above 100 MW, in general. The single-reheat tandem (same-shaft) steam turbine is shown in Figure 3.3. There are three stages in Figure 3.3: HP, IP, and LP. After passing through the MSVs and GVs, the high-pressure steam flows through the high-pressure stage where it experiences a partial expansion. Subsequently, the steam is guided back to the boiler and reheated in the heat exchanger to increase its enthalpy. From the reheater, the steam flows through the reheat emergency stop valve

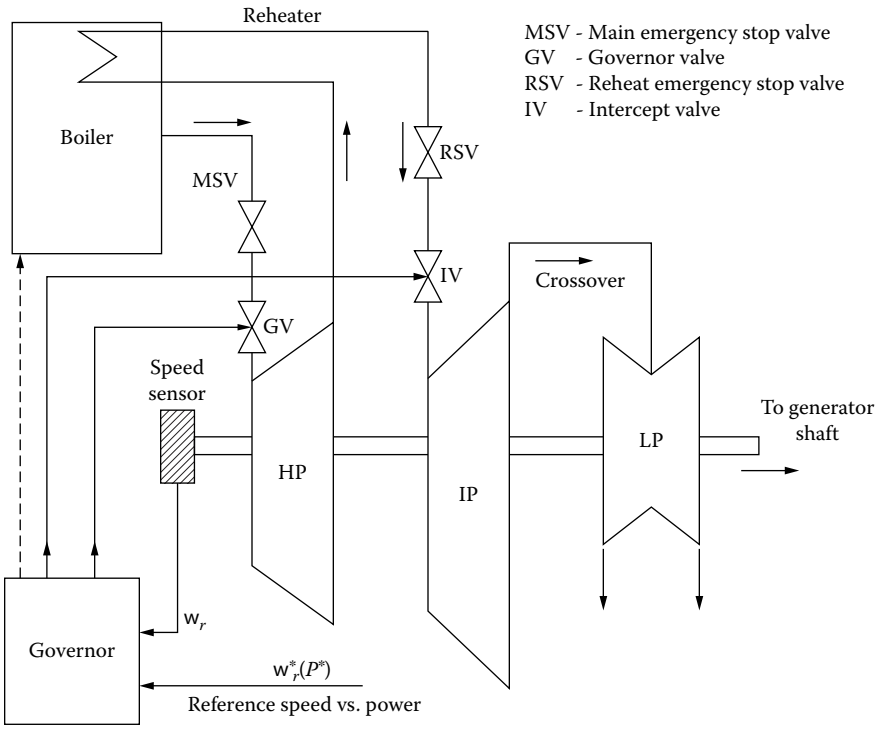

FIGURE 3.3 Single-reheat tandem-compound steam turbine.

(RSV) and intercept valve (IV) to the intermediate-pressure stage of the turbine, where again it expands to do mechanical work. For final expansion, the steam is headed to the crossover pipes and through the low pressure stage where more mechanical work is done. Typically, the power of the turbine is divided as follows: 30% in the HP, 40% in the IP, and 30% in the LP stages. The governor controls both the GV in the HP stage and the IV in the IP stage to provide fast and safe control.

During steam turbine starting — toward synchronous generator synchronization — the MSV is fully open, while the GV and IV are controlled by the governor system to regulate the speed and power. The governor system contains a hydraulic (oil) or an electrohydraulic servomotor to operate the GV and IV and to control the fuel and air mix admission and its parameters in the boiler. The MSV and RSV are used to quickly and safely stop the turbine under emergency conditions.

Turbines with one shaft are called tandem compound, while those with two shafts (eventually at different speeds) are called cross-compound. In essence, the LP stage of the turbine is attributed to a separate shaft (Figure 3.4). Controlling the speeds and powers of two shafts is difficult, though it adds flexibility. Also, shafts are shorter. Tandem-compound (single-shaft) configurations are more often used.

Nuclear units generally have tandem-compound (single-shaft) configurations and run at 1800 (1500) rpm for 60 (50) Hz power systems. They contain one HP and three LP stages (Figure 3.5). The HP exhaust passes through the moisture reheater (MSR) before entering the LP 1,2,3 stages in order to reduce steam moisture losses and erosion. The HP exhaust is also reheated by the HP steam flow.

The governor acts upon the GV and the IV 1,2,3 to control the steam admission in the HP and LP 1,2,3 stages, while the MSV and the RSV 1,2,3 are used only for emergency tripping of the turbine. In general, the GVs (control) are of the plug-diffuser type, while the IVs may be either the plug or the butterfly type (Figure 3.6a and Figure 3.6b, respectively). The valve characteristics are partly nonlinear, and, for better control, they are often "linearized" through the control system.

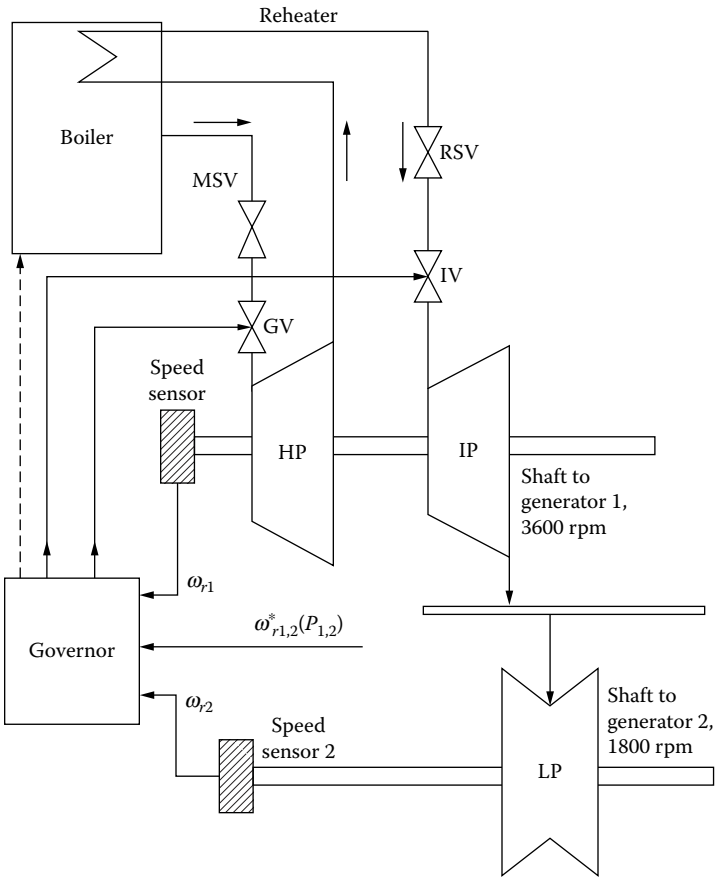

FIGURE 3.4 Single-reheat cross-compound (3600/1800 rpm) steam turbine.

3.3 Steam Turbine Modeling

The complete model of a multiple-stage steam turbine is rather involved. This is why we present here first the simple steam vessel (boiler, reheated) model (Figure 3.7), [1–3], and derive the power expression for the single-stage steam turbine.

The mass continuity equation in the vessel is written as follows:

$$\frac{dW}{dt} = V\frac{d\rho}{dt} = Q_{input} - Q_{output} \tag{3.1}$$

where

V = the volume (m^3)
Q = the steam mass flow rate (kg/sec)
ρ = the density of steam (kg/m^3)
W = the weight of the steam in the vessel (kg).

Let us assume that the flow rate out of the vessel Q_{output} is proportional to the internal pressure in the vessel:

$$Q_{output} = \frac{Q_0}{P_0} P \tag{3.2}$$

where

P = the pressure (KPa)

P_0 and Q_0 = the rated pressure and flow rate out of the vessel

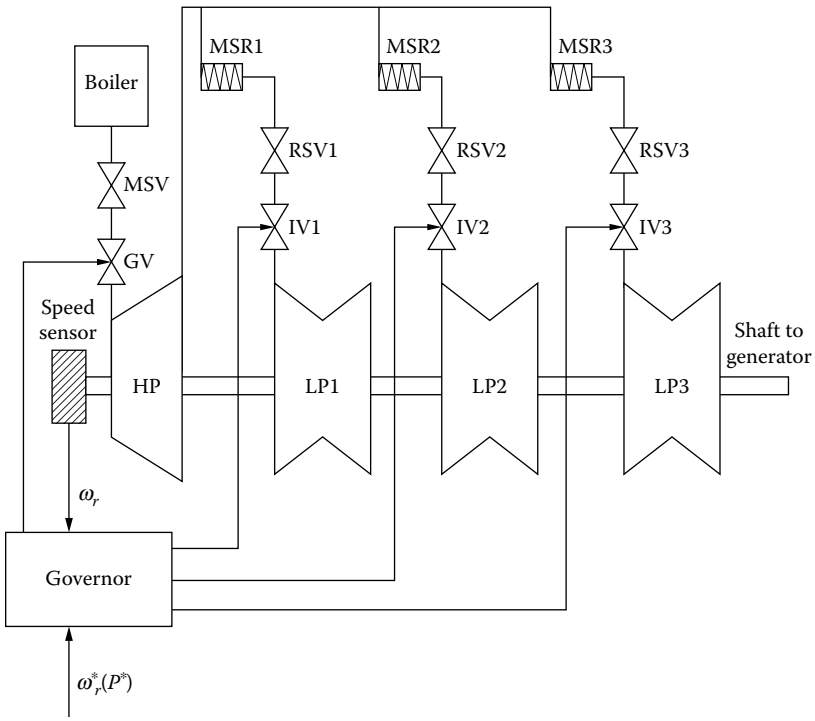

FIGURE 3.5 Typical nuclear steam turbine.

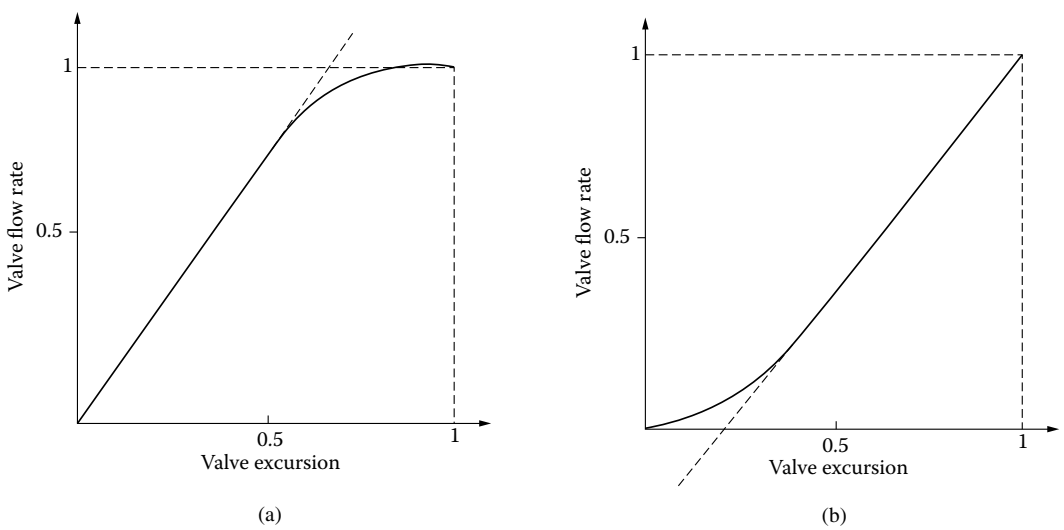

FIGURE 3.6 Steam valve characteristics: (a) plug-diffuser valve and (b) butterfly-type valve.

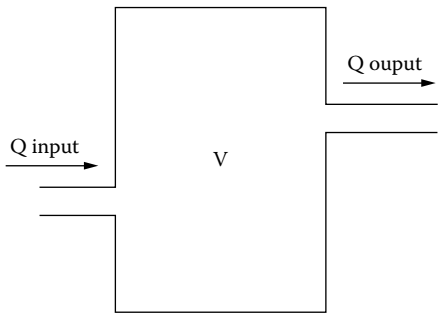

FIGURE 3.7 The steam vessel.

As the temperature in the vessel may be considered constant,

$$\frac{d\rho}{dt} = \frac{\partial \rho}{\partial P} \cdot \frac{dP}{dt} \tag{3.3}$$

Steam tables provide $(\partial \rho / \partial P)$ functions.
Finally, from Equation 3.1 through Equation 3.3, we obtain the following:

$$Q_{input} - Q_{output} = T_V \frac{dQ_{output}}{dt} \tag{3.4}$$

$$T_V = \frac{P_0}{Q_0} V \cdot \frac{\partial \rho}{\partial P} \tag{3.5}$$

T_V is the time constant of the steam vessel. With $d/dt = s$, the Laplace form of Equation 3.4 can be written as follows:

$$\frac{Q_{output}}{Q_{input}} = \frac{1}{1 + T_V \cdot s} \tag{3.6}$$

The first-order model of the steam vessel has been obtained. The shaft torque T_m in modern steam turbines is proportional to the flow rate:

$$T_m = K_m \cdot Q \tag{3.7}$$

So the power P_m is:

$$P_m = T_m \cdot \Omega_m = K_m Q \cdot 2\pi n_m \tag{3.8}$$

Example 3.1

The reheater steam volume of a steam turbine is characterized by $Q_0 = 200$ kg/sec, $V = 100$ m^3, $P_0 = 4000$ kPa, and $\partial \rho / \partial P = 0.004$.

Calculate the time constant T_R of the reheater and its transfer function.

We use Equation 3.4 and Equation 3.5 and, respectively, Equation 3.6:

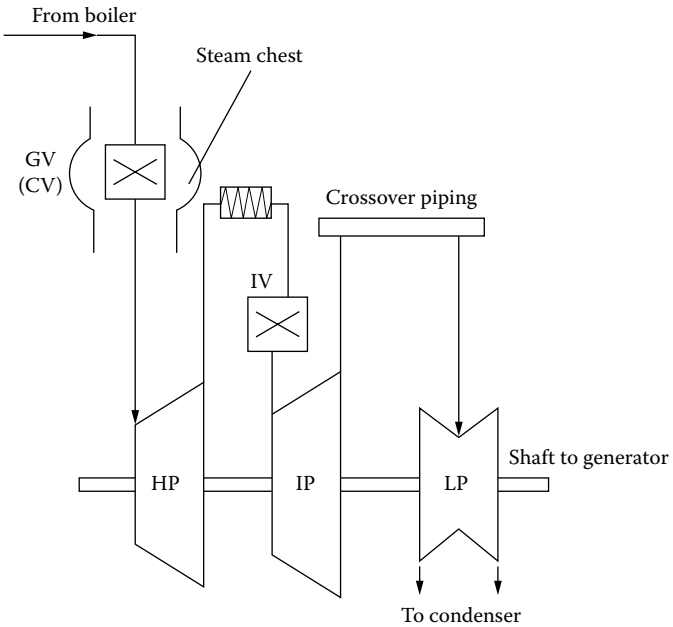

FIGURE 3.8 Single-reheat tandem-compound steam turbine.

$$T_R = \frac{P_0}{Q_0} V \cdot \frac{\partial \rho}{\partial P} = \frac{4000}{200} \times 100 \times 0.004 = 8.0 \text{ sec}$$

$$\frac{Q_{output}}{Q_{input}} = \frac{1}{1 + 8 \cdot s}$$

Now consider the rather complete model of a single-reheat, tandem-compound steam turbine (Figure 3.3). We will follow the steam journey through the turbine, identifying a succession of time delays/time constants.

The MSV and RSV are not shown in Figure 3.8, as they intervene only in emergency conditions.

The GVs modulate the steam flow through the turbine to provide for the required (reference) load (power)/frequency (speed) control. The GV has a steam chest where substantial amounts of steam are stored; and it is also found in the inlet piping. Consequently, the response of steam flow to a change in a GV opening exhibits a time delay due to the charging time of the inlet piping and steam chest. This time delay is characterized by a time constant T_{CH} in the order of 0.2 to 0.3 sec.

The IVs are used for rapid control of mechanical power (they handle 70% of power) during overspeed conditions; thus, their delay time may be neglected in a first approximation.

The steam flow in the IP and LP stages may be changed with an increase in pressure in the reheater. As the reheater holds a large amount of steam, its response-time delay is larger. An equivalent larger time constant T_{RM} of 5 to 10 sec is characteristic of this delay [4].

The crossover piping also introduces a delay that may be characterized by another time constant T_{CO}.

We should also consider that the HP, IP, and LP stages produce F_{HP}, F_{IP}, and F_{LP} fractions of total turbine power such that

$$F_{HP} + F_{IP} + F_{LP} = 1 \tag{3.9}$$

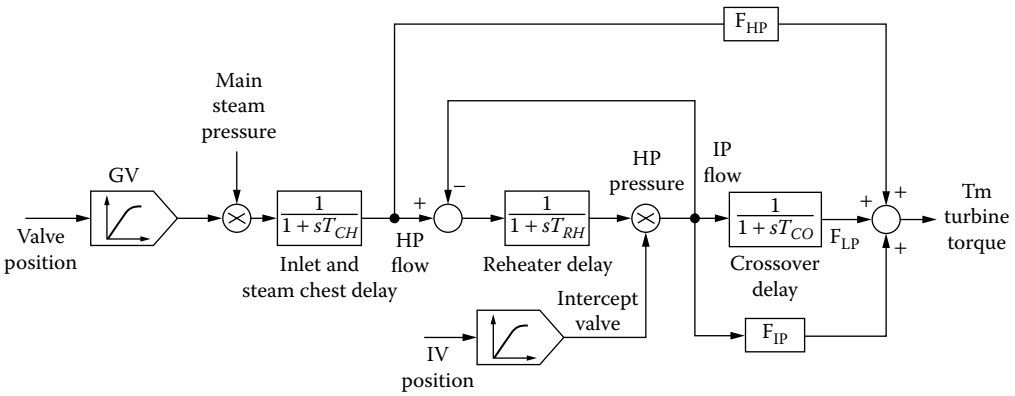

FIGURE 3.9 Structural diagram of single-reheat tandem-compound steam turbine.

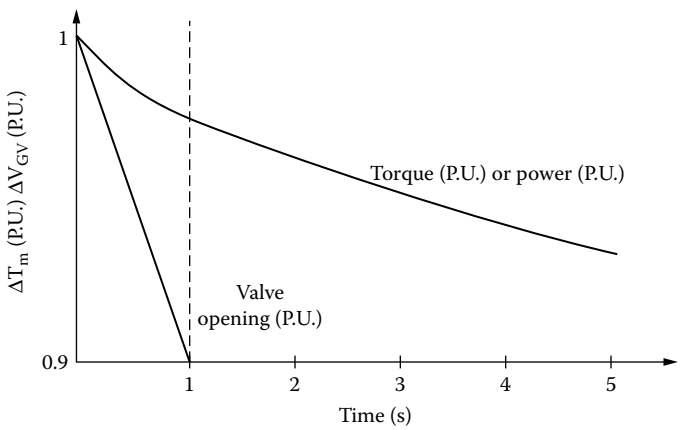

FIGURE 3.10 Steam turbine response to 0.1 (P.U.) 1 sec ramp change of GV opening.

We may integrate these aspects of a steam turbine model into a structural diagram as shown in Figure 3.9.

Typically, as already stated: $F_{HP} = F_{IP} = 0.3$, $F_{LP} = 0.4$, $T_{CH} \approx 0.2$–0.3 sec, $T_{RH} = 5$–9 sec, and $T_{CO} = 0.4$–0.6 sec.

In a nuclear-fuel steam turbine, the IP stage is missing ($F_{IP} = 0$, $F_{LP} = 0.7$), and T_{RH} and T_{CH} are notably smaller. As T_{CH} is largest, reheat turbines tend to be slower than nonreheat turbines. After neglecting T_{CO} and considering GV as linear, the simplified transfer function may be obtained:

$$\frac{\Delta Tm}{\Delta V_{GV}} \approx \frac{\left(1+sF_{HP}T_{RH}\right)}{\left(1+sT_{CH}\right)\left(1+sT_{RH}\right)} \tag{3.10}$$

The transfer function in Equation 3.10 clearly shows that the steam turbine has a straightforward response to GV opening.

A typical response in torque (in per unit, P.U.) — or in power — to 1 sec ramp of 0.1 (P.U.) change in GV opening is shown in Figure 3.10 for $T_{CH} = 8$ sec, $F_{HP} = 0.3$, and $T_{CH} = T_{CO} = 0$.

In enhanced steam turbine models involving various details, such as IV, more rigorous representation counting for the (fast) pressure difference across the valve may be required to better model various intricate transient phenomena.

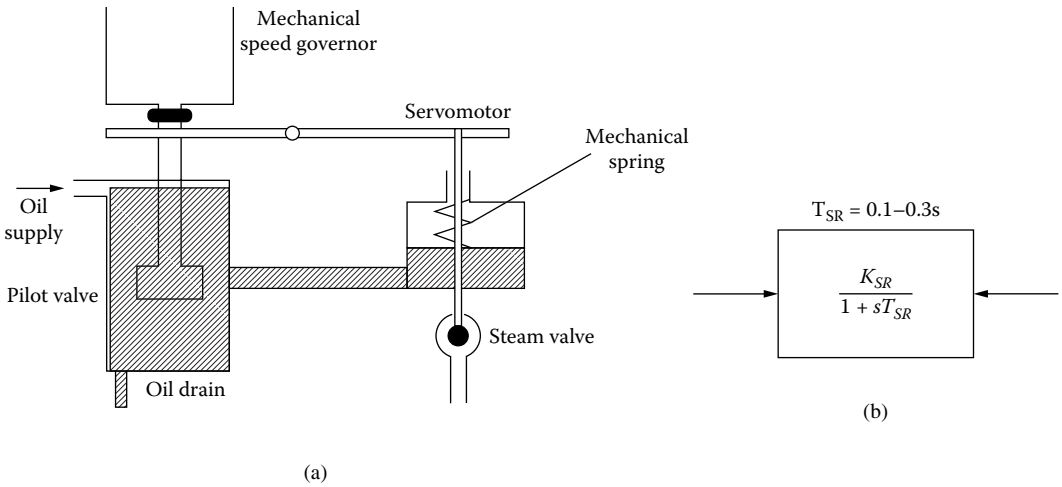

FIGURE 3.11 Speed relay: (a) configuration and (b) transfer function.

3.4 Speed Governors for Steam Turbines

The governor system of a turbine performs a multitude of functions, including the following [1–4]:

- Speed (frequency)/load (power) control: mainly through GVs
- Overspeed control: mainly through the IV
- Overspeed trip: through MSV and RSV
- Start-up and shutdown control

The speed/load (frequency/power) control (Figure 3.2) is achieved through the control of the GV to provide linearly decreasing speed with load, with a small speed drop of 3 to 5%. This function allows for paralleling generators with adequate load sharing. Following a reduction in electrical load, the governor system has to limit overspeed to a maximum of 120%, in order to preserve turbine integrity. Reheat-type steam turbines have two separate valve groups (GV and IV) to rapidly control the steam flow to the turbine.

The objective of the overspeed control is set to about 110 to 115% of rated speed to prevent overspeed tripping of the turbine in case a load rejection condition occurs.

The emergency tripping (through MSV and RSV — Figure 3.3 and Figure 3.5) is a protection solution in case normal and overspeed controls fail to limit the speed to below 120%.

A steam turbine is provided with four or more GVs that admit steam through nozzle sections distributed around the periphery of the HP stage. In normal operation, the GVs are open sequentially to provide better efficiency at partial load. During the start-up, all the GVs are fully open, and stop valves control steam admission.

Governor systems for steam turbines evolve continuously. Their evolution mainly occurred from mechanical-hydraulic systems to electrohydraulic systems [4].

In some embodiments, the main governor systems activate and control the GV, while an auxiliary governor system operates and controls the IV [4]. A mechanical-hydraulic governor generally contains a centrifugal speed governor (controller), that has an effect that is amplified through a speed relay to open the steam valves. The speed relay contains a pilot valve (activated by the speed governor) and a spring-loaded servomotor (Figure 3.11a and Figure 3.11b).

In electrohydraulic turbine governor systems, the speed governor and speed relay are replaced by electronic controls and an electric servomotor that finally activates the steam valve.

In large turbines an additional level of energy amplification is needed. Hydraulic servomotors are used for the scope (Figure 3.12). By combining the two stages — the speed relay and the hydraulic servomotor — the basic turbine governor is obtained (Figure 3.13).

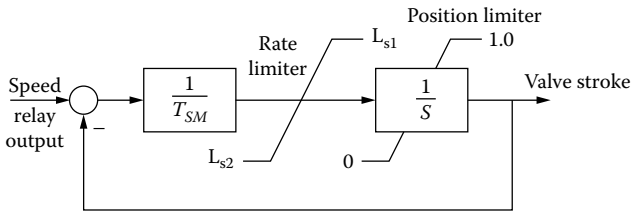

FIGURE 3.12 Hydraulic servomotor structural diagram.

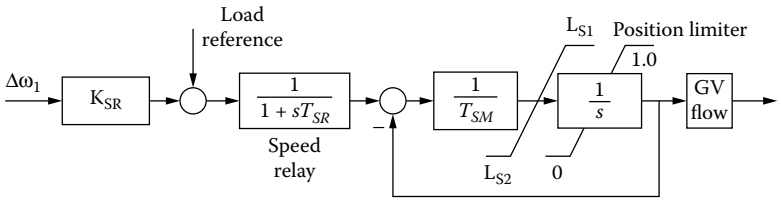

FIGURE 3.13 Basic turbine governor.

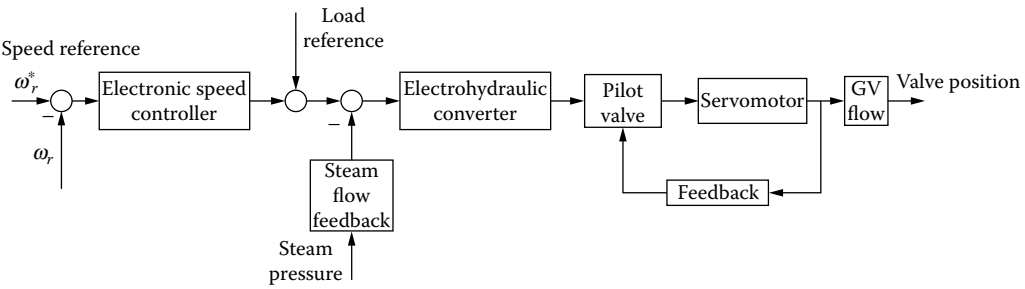

FIGURE 3.14 Generic electrohydraulic governing system.

For a speed drop of 4% at rated power, $K_{SR} = 25$ (Figure 3.12). A similar structure may be used to control the IV [2].

Electrohydraulic governor systems perform similar functions, but by using electronics control in the lower power stages, they bring more flexibility, and a faster and more robust response. They are provided with acceleration detection and load power unbalance relay compensation. The structure of a generic electrohydraulic governor system is shown in Figure 3.14. Notice the two stages in actuation: the electrohydraulic converter plus the servomotor, and the electronic speed controller.

The development of modern nonlinear control (adaptive, sliding mode, fuzzy, neural networks, H_∞, etc.) [5] led to the recent availability of a wide variety of electronic speed controllers or total steam turbine-generator controllers [6]. These, however, fall beyond the scope of our discussion here.

3.5 Gas Turbines

Gas turbines burn gas, and that thermal energy is then converted into mechanical work. Air is used as the working fluid. There are many variations in gas turbine topology and operation [1], but the most used one seems to be the open regenerative cycle type (Figure 3.15).

The gas turbine in Figure 3.14 consists of an air compressor (C) driven by the turbine (T) and the combustion chamber (CH). The fuel enters the combustion chamber through the GV, where it is mixed with the hot-compressed air from the compressor. The combustion product is then directed into the turbine, where it expands and transfers energy to the moving blades of the gas turbine. The exhaust gas heats the air from the compressor in the heat exchanger. The typical efficiency of a gas turbine is 35%.

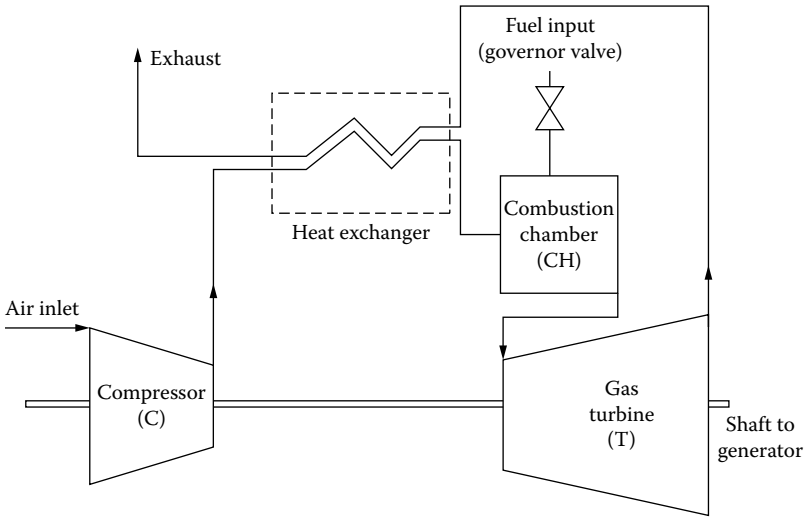

FIGURE 3.15 Open regenerative cycle gas turbine.

More complicated cycles, such as compressor intercooling and reheating or intercooling with regeneration and recooling, are used for further (slight) improvements in performance [1].

The combined- and steam-cycle gas turbines were recently proven to deliver an efficiency of 55% or even slightly more. The generic combined-cycle gas turbine is shown in Figure 3.16.

The exhaust heat from the gas turbine is directed through the heat recovery boiler (HRB) to produce steam, which, in turn, is used to produce more mechanical power through a steam turbine section on the same shaft. With the gas exhaust exiting the gas turbine above 500 C and supplementary fuel burning, the HRB temperature may rise further than the temperature of the HP steam, thus increasing efficiency. Additionally, some steam for home (office) heating or process industries may be delivered.

Already in the tens of MW, combined-cycle gas turbines are becoming popular for cogeneration in distributed power systems in the MW or even tenths and hundreds of kilowatts per unit. Besides efficiency, the short construction time, low capital cost, low SO_2 emission, little staffing necessary, and easy fuel (gas) handling are all main merits of combined-cycle gas turbines. Their construction at very high speeds (tens of krpm) up to the 10 MW range, with full-power electronics between the generator and the distributed power grid, or in stand-alone operation mode at 50(60) Hz, make the gas turbines a way of the future in this power range.

3.6 Diesel Engines

Distributed electric power systems, with distribution feeders at approximately 12 kV, standby power sets ready for quick intervention in case of emergency or on vessels, locomotives, or series or parallel hybrid vehicles, and power-leveling systems in tandem with wind generators, all make use of diesel (or internal combustion) engines as prime movers for their electric generators. The power per unit varies from a few tenths of a kilowatt to a few megawatts.

As for steam or gas turbines, the speed of a diesel-engine generator set is controlled through a speed governor. The dynamics and control of fuel–air mix admission are very important to the quality of the electric power delivered to the local power grid or to the connected loads, in stand-alone applications.

3.6.1 Diesel-Engine Operation

In four-cycle internal combustion engines [7], and the diesel engine is one of them, with the period of one shaft revolution $T_{REV} = 1/n$ (n is the shaft speed in rev/sec), the period of one engine power stroke T_{PS} is

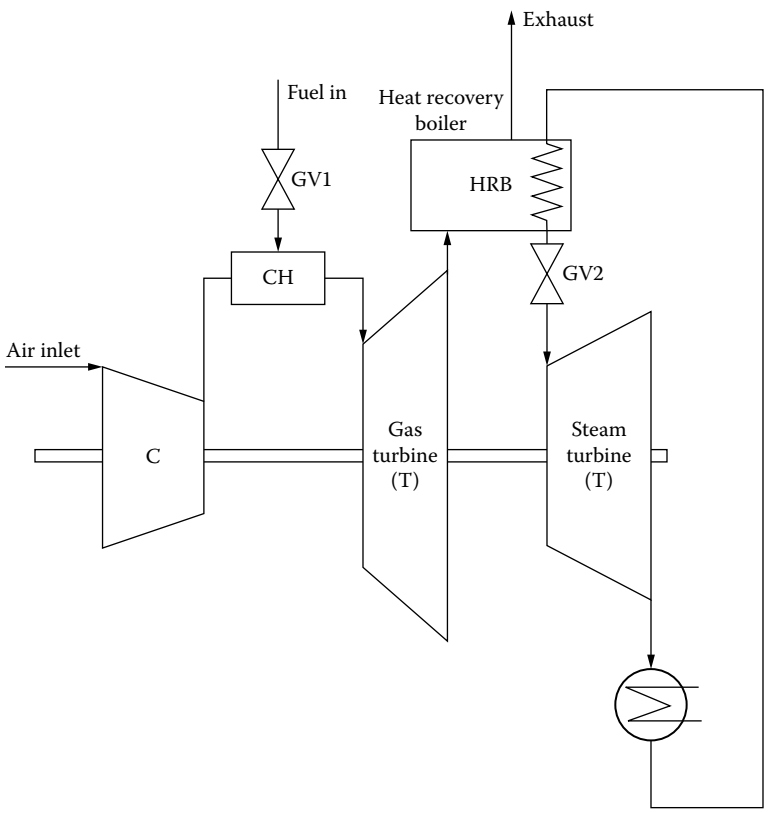

FIGURE 3.16 Combined-cycle unishaft gas turbine.

$$T_{PS} = 2T_{REV} \tag{3.11}$$

The frequency of power stroke f_{PS} is as follows:

$$f_{PS} = \frac{1}{T_{PS}} \tag{3.12}$$

For an engine with N_c cylinders, the number of cylinders that fire each revolution, N_f, is

$$N_f = \frac{N_c}{2} \tag{3.13}$$

The cylinders are arranged symmetrically on the crankshaft, so that the firing of the N_f cylinders is uniformely spaced in angle terms. Consequently, the angular separation (θ_c) between successive firings in a four-cycle engine is as follows:

$$\theta_c = \frac{720^0}{N_c} \tag{3.14}$$

The firing angles for a twelve-cylinder diesel engine are illustrated in Figure 3.17a, while the two-revolution sequence is intake (I), compression (C), power (P), and exhaust (E) (Figure 3.17b). The twelve-

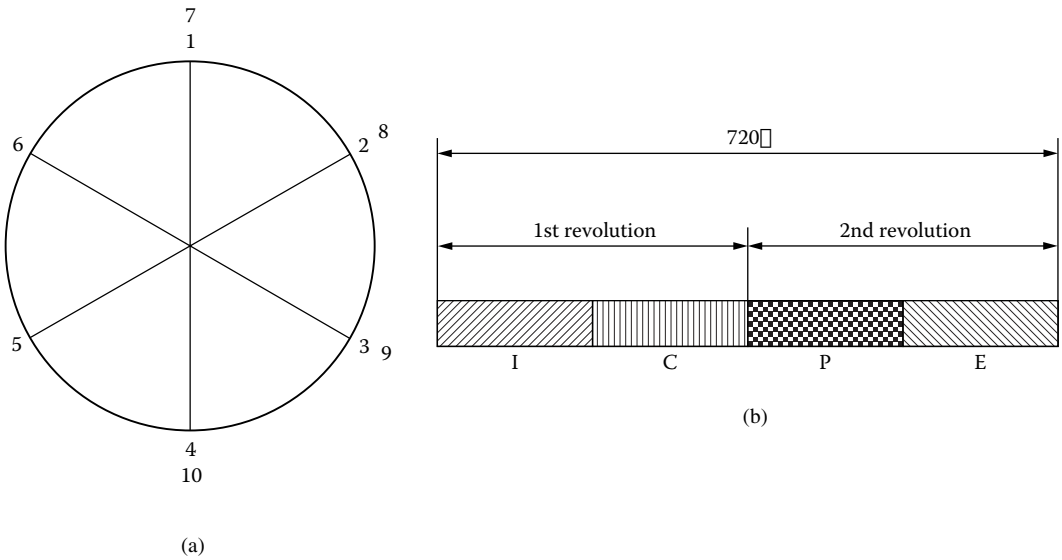

FIGURE 3.17 Twelve-cylinder four-cycle diesel engine: (a) configuration and (b) sequence.

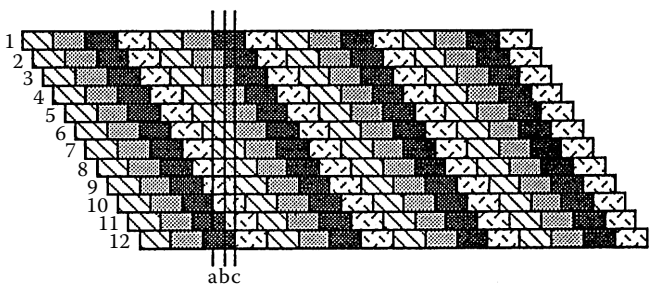

FIGURE 3.18 Twelve-cylinder engine timing.

cylinder timing is shown in Figure 3.18. There are three cylinders out of twelve firing simultaneously at steady state. The resultant shaft torque of one cylinder varies with shaft angle, as shown in Figure 3.19. The compression torque is negative, while during the power cycle, it is positive. With twelve cylinders, the torque will have much smaller pulsations, with twelve peaks over 720 (period of power engine stroke) — see Figure 3.20. Any misfire in one or a few of the cylinders would produce severe pulsations in the torque that would reflect as a flicker in the generator output voltage [8].

Large diesel engines generally have a turbocharger (Figure 3.21) that notably influences the dynamic response to perturbations by its dynamics and inertia [9]. The turbocharger is essentially an air compressor that is driven by a turbine that runs on the engine exhaust gas. The compressor provides compressed air to the engine cylinders. The turbocharger works as an energy recovery device with about 2% power recovery.

3.6.2 Diesel-Engine Modeling

A diagram of the general structure of a diesel engine with turbocharger and control is presented in Figure 3.22.

The following are the most important components:

- The actuator (governor) driver that appears as a simple gain K_3.

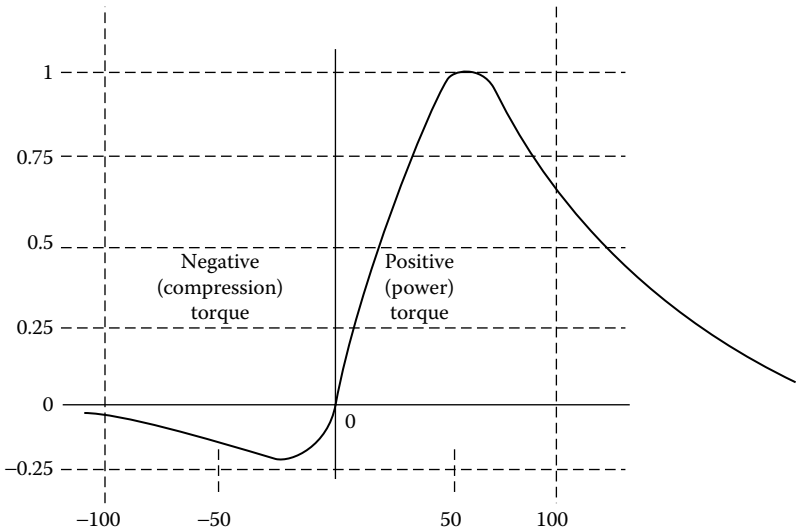

FIGURE 3.19 P.U. torque/angle for one cylinder.

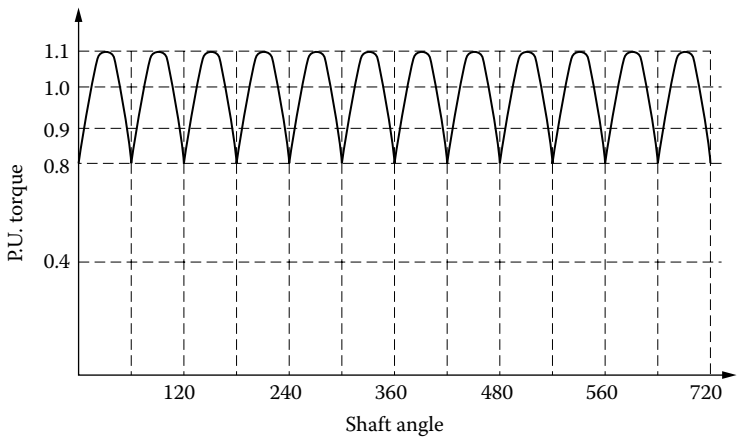

FIGURE 3.20 P.U. torque vs. shaft angle in a 12-cylinder ICE (internal combustion engine).

- The actuator (governor) fuel controller that converts the actuator's driver into an equivalent fuel flow, **Φ**. This actuator is represented by a gain K_2 and a time constant (delay) τ_2, which is dependent on oil temperature, and an aging-produced backlash.
- The inertias of engine J_E, turbocharger J_T, and electric generator (alternator) J_G.
- The flexible coupling that mechanically connects the diesel engine to the alternator (it might also contain a transmission).
- The diesel engine is represented by the steady-state gain K_1 — constant for low fuel flow **Φ** and saturated for large **Φ**, multiplied by the equivalence ratio factor (erf) and by a time constant τ_1.
- The erf depends on the engine equivalence ratio (eer), which, in turn, is the ratio of fuel/air normalized by its stoichiometric value. A typical variation of erf with eer is shown in Figure 3.22. In essence, erf is reduced, because when the ratio of fuel/air increases, incomplete combustion occurs, leading to low torque and smoky exhaust.
- The dead time of the diesel engine is composed of three delays: the time elapsed until the actuator output actually injects fuel into the cylinder, fuel burning time to produce torque, and time until all cylinders produce torque at the engine shaft:

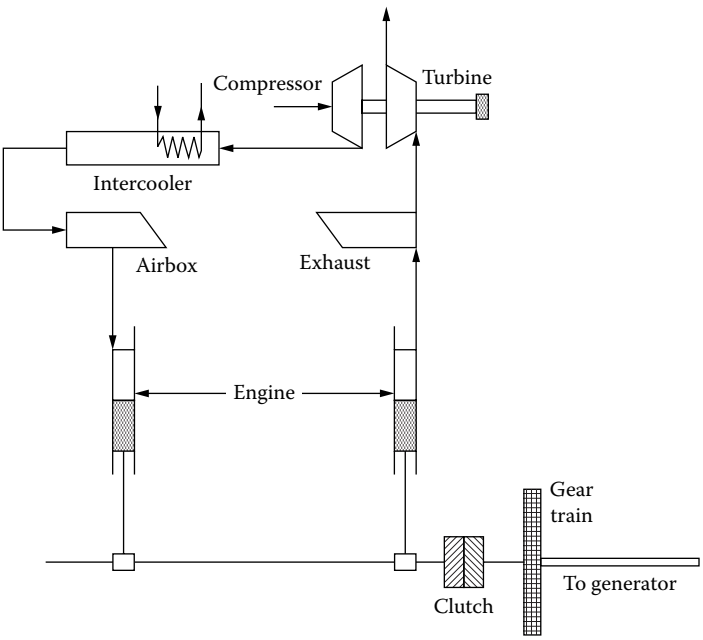

FIGURE 3.21 Diesel engine with turbocharger.

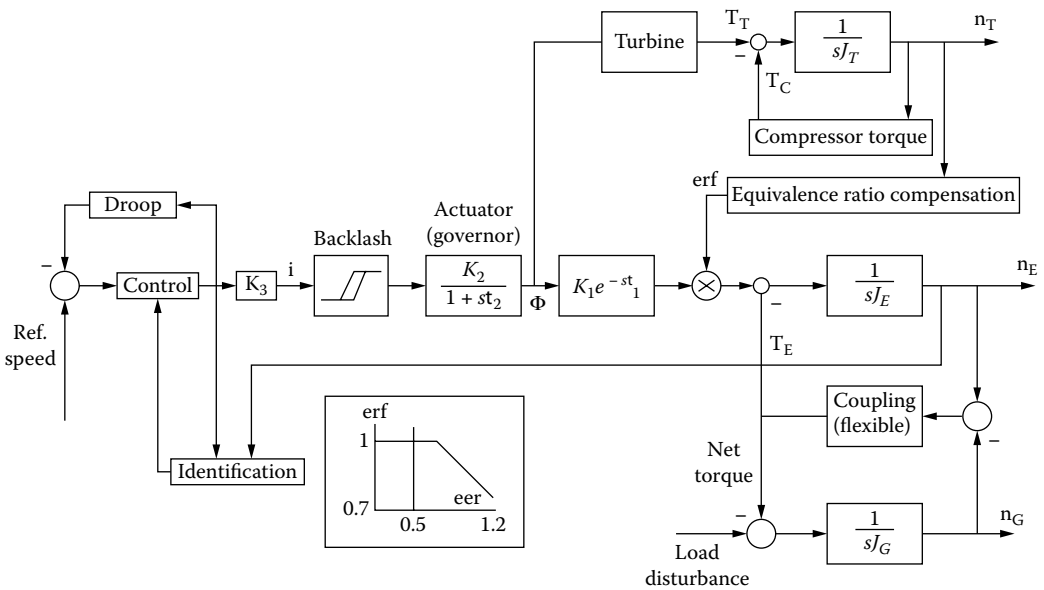

FIGURE 3.22 Diesel engine with turbocharger and controller.

$$\tau_1 \approx A + \frac{B}{n_E} + \frac{C}{n_E^2} \tag{3.15}$$

where n_E is the engine speed.

The turbocharger acts upon the engine in the following ways:

- It draws energy from the exhaust to run its turbine; the more fuel in the engine, the more exhaust is available.
- It compresses air at a rate that is a nonlinear function of speed; the compressor is driven by the turbine, and thus, the turbine speed and ultimate erf in the engine are influenced by the airflow rate.
- The turbocharger runs freely at high speed, but it is coupled through a clutch to the engine at low speeds, to be able to supply enough air at all speeds; thus, the system inertia changes at low speeds, by including the turbocharger inertia.

Any load change leads to transients in the system pictured in Figure 3.22 that may lead to oscillations due to the nonlinear effects of fuel–air flow — equivalence ratio factor — inertia. As a result, there will be either too little or too much air in the fuel mix. In the first case, smoky exhaust will be apparent. In the second situation, not enough torque will be available for the electric load, and the generator may pull out of synchronism. This situation indicates that proportional integral (PI) controllers of engine speed are not adequate, and nonlinear controllers (adaptive, variable structure, etc.) are required [10].

A higher-order model may be adopted both for the actuator [11, 12] and for the engine [13] to better simulate in detail the diesel-engine performance for transients and control.

3.7 Stirling Engines

Stirling engines are part of the family of thermal engines: steam turbines, gas turbines, spark-ignited engines, and diesel engines. They were already described briefly in this chapter, but it is time now to dwell a little on the thermodynamic engine cycles to pave the way for our discussion on Stirling engines.

3.7.1 Summary of Thermodynamic Basic Cycles

The steam engine, invented by James Watt, is a continuous combustion machine. Subsequently, the steam is directed from the boiler to the cylinders (Figure 3.23a and Figure 3.23b). The typical four steps of the steam engine (Figure 3.23a) are as follows:

- Isochoric compression (1–1′) followed by isothermal expansion (1′–2): The hot steam enters the cylinder through the open valve at constant volume; it then expands at constant temperature.
- Isotropic expansion: Once the valve is closed, the expansion goes on until the maximum volume is reached (3).
- Isochoric heat regeneration (3–3) and isothermal compression (3′–4): The pressure drops at constant volume, and then the steam is compressed at constant temperature.
- Isentropic compression takes place after the valve is closed and the gas is mechanically compressed. An approximate formula for thermal efficiency η_{th} is as follows [13]:

$$\eta_{th} = 1 - \frac{\rho^{K-1}(K-1)(1+\ln\rho)}{\varepsilon^{K-1}(x-1)+(K-1)\ln\rho} \tag{3.16}$$

where

$\varepsilon = V_3/V_1$ is the compression ratio
$\rho = V_2/V_1 = V_3/V_4$ is the partial compression ratio
$x = p_1'/p_1$ is the pressure ratio

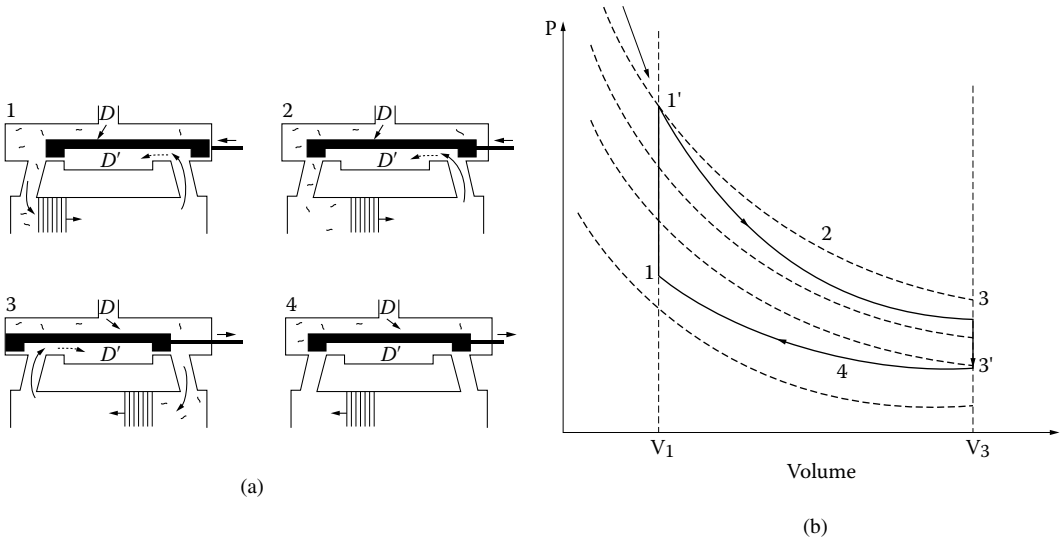

FIGURE 3.23 The steam engine "cycle": (a) the four steps and (b) PV diagram.

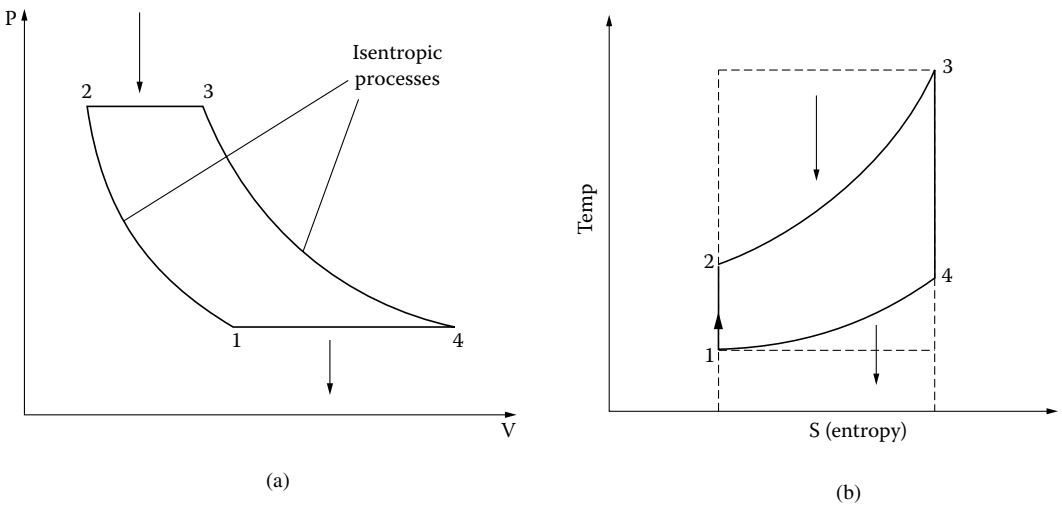

FIGURE 3.24 Brayton cycle for gas turbines: (a) PV diagram and (b) TS diagram.

For $\rho = 2$, $x = 10$, $K = 1.4$, and $\varepsilon = 3$, $\eta_{th} = 31\%$.

The gas turbine engine fuel is also continuously combusted in combination with precompressed air. The gas expansion turns the turbine shaft to produce mechanical power. The gas turbines work on a Brayton cycle (Figure 3.24a and Figure 3.24b). The four steps of a Brayton cycle are as follows:

- Isentropic compression
- Isobaric input of thermal energy
- Isentropic expansion (work generation)
- Isobaric thermal energy loss

Similarly, with $T_1/T_4 = T_2/T_3$ for the isentropic steps, and the injection ratio $\rho = T_3/T_2$, the thermal efficiency η_{th} is as follows:

$$\eta_{th} \approx 1 - \frac{1}{\rho}\frac{T_4}{T_2} \tag{3.17a}$$

With ideal, complete, heat recirculation:

$$\eta_{th} \approx 1 - \frac{1}{\rho} \tag{3.17b}$$

Gas turbines are more compact than other thermal machines; they are easy to start and have low vibration, but they also have low efficiency at low loads (ρ small) and tend to have poor behavior during transients.

The spark-ignition (Otto) engines work on the cycle shown in Figure 3.25a and Figure 3.25b. The four steps are as follows:

- Isentropic compression
- Isochoric input of thermal energy
- Isentropic expansion (kinetic energy output)
- Isochoric heat loss

The ideal thermal efficiency η_{th} is

$$\eta_{th} = 1 - \frac{1}{\varepsilon^{K-1}}; \varepsilon = V_1 / V_2 \tag{3.18}$$

where

$$\frac{T_4}{T_3} = \frac{T_1}{T_2} = \left(\frac{V_3}{V_4}\right)^{K-1} = \frac{1}{\varepsilon^{K-1}} \tag{3.19}$$

for isentropic processes. With a high compression ratio (say $\varepsilon = 9$) and the adiabatic coefficient K = 1.5, $\eta_{th} = 0.66$.

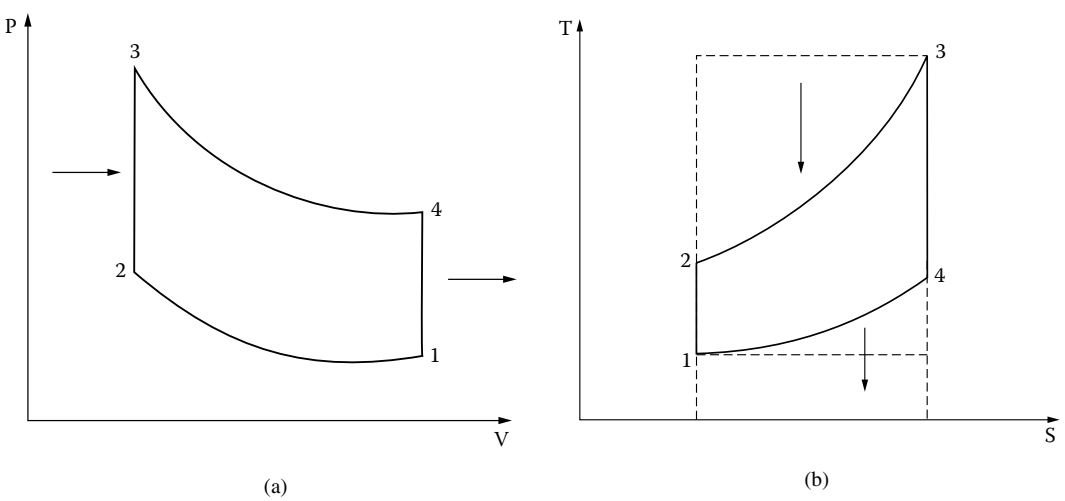

FIGURE 3.25 Spark-ignition engines: (a) PV diagram and (b) TS diagram.

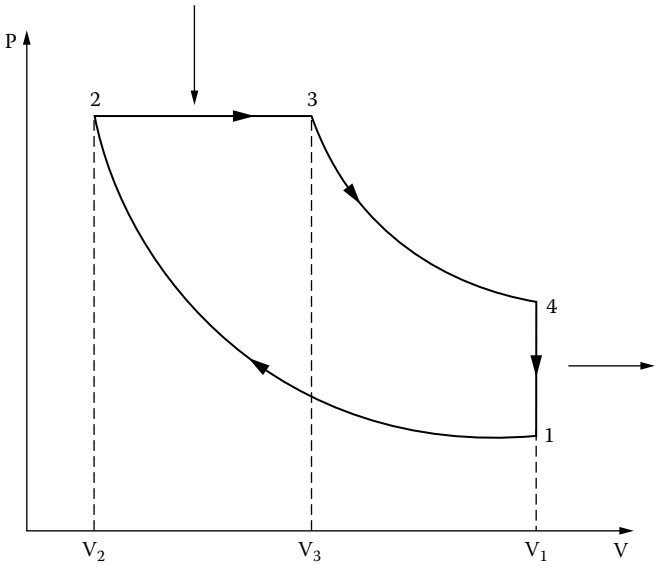

FIGURE 3.26 The diesel-engine cycle.

The diesel-engine cycle is shown in Figure 3.26. During the downward movement of the piston, an isobaric state change takes place by controlled injection of fuel:

$$\rho = \frac{V_3}{V_2} = \frac{T_3}{T_2};$$
$$\eta_{th} = 1 - \frac{1}{\varepsilon^{K-1}} \cdot \frac{1}{K} \frac{\rho^K - 1}{\rho - 1} \tag{3.20}$$

Efficiency decreases when load ρ increases, in contrast to spark-ignition engines for the same ε. Lower compression ratios (ε) than those for spark-ignition engines are characteristic of diesel engines so as to obtain higher thermal efficiency.

3.7.2 The Stirling-Cycle Engine

The Stirling engine (developed in 1816) is a piston engine with continuous heat supply (Figure 3.27a through Figure 3.27c). In some respects, the Stirling cycle is similar to the Carnot cycle (with its two isothermal steps). It contains two opposed pistons and a regenerator in between. The regenerator is made in the form of strips of metal. One of the two volumes is the expansion space kept at a high temperature T_{max}, while the other volume is the compression space kept at a low temperature T_{min}. Thermal axial conduction is considered negligible. Suppose that the working fluid (all of it) is in the cold compression space.

During compression (steps 1 to 2), the temperature is kept constant because heat is extracted from the compression space cylinder to the surroundings.

During the transfer step (steps 2 to 3), both pistons move simultaneously; the compression piston moves toward the regenerator, while the expansion piston moves away from it. So, the volume stays constant. The working fluid is, consequently, transferred through the porous regenerator from compression to expansion space and is heated from T_{min} to T_{max}. An increase in pressure also takes place between steps 2 and 3. In the expansion step (3 to 4), the expansion piston still moves away from the regenerator, but the compression piston stays idle at an inner dead point. The pressure decreases, and the volume

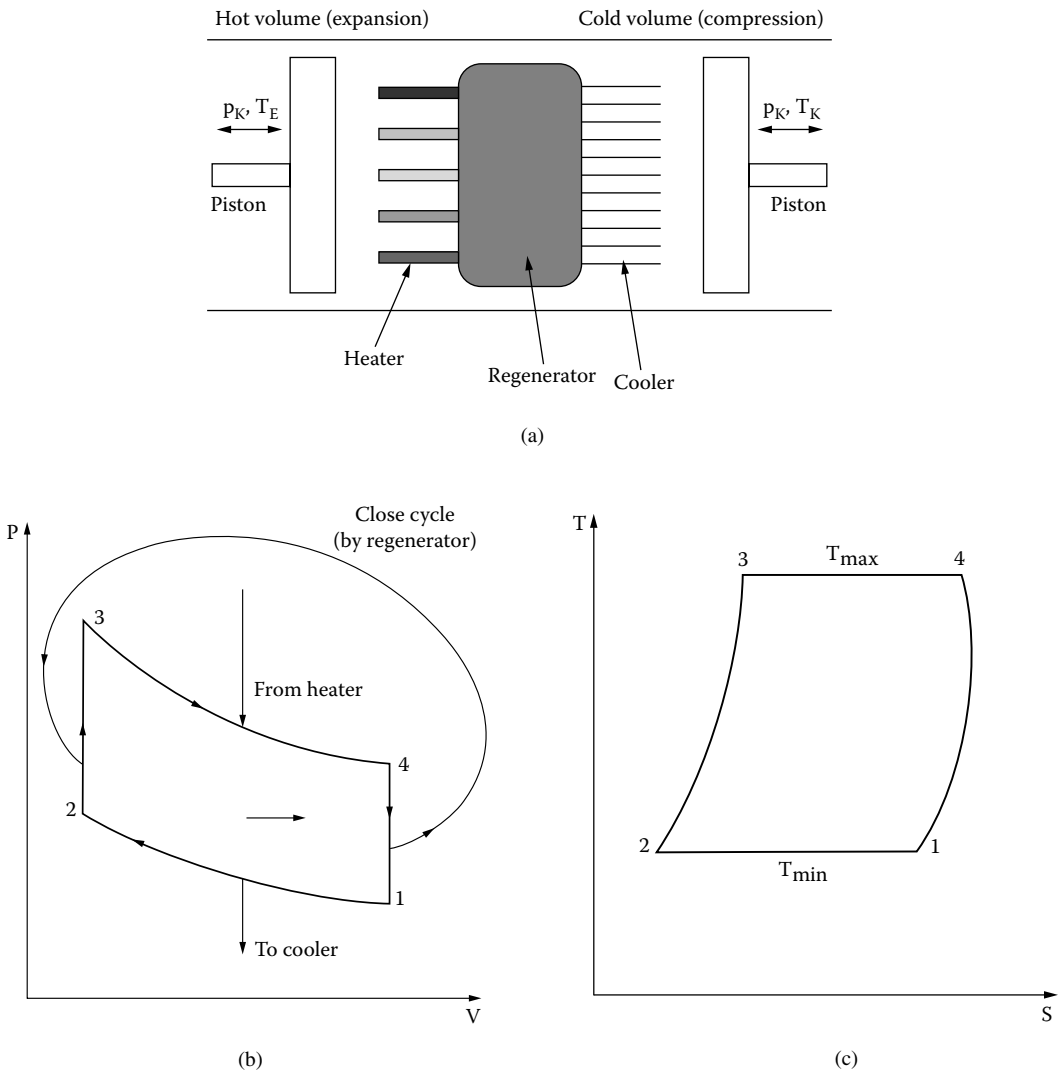

FIGURE 3.27 The Stirling engine: (a) mechanical representation and (b) and (c) the thermal cycle.

increases, but the temperature stays constant, because heat is added from an external source. Then, again, a transfer step (step 4 to step 1) occurs, with both pistons moving simultaneously to transfer the working fluid (at constant volume) through the regenerator from the expansion to the compression space. Heat is transferred from the working fluid to the regenerator, which cools at $T_{\min}$ in the compression space.

The ideal thermal efficiency η_{th} is as follows:

$$\eta_{th}^{i} = 1 - \frac{T_{\min}}{T_{\max}} \tag{3.21}$$

So, it is heavily dependent on the maximum and minimum temperatures, as is the Carnot cycle. Practical Stirling-type cycles depart from the ideal. The practical efficiency of Stirling-cycle engines is much lower: $\eta_{th} < \eta_{th} K_{th}$ ($K_{th} < 0.5$, in general).

Stirling engines may use any heat source and can use various working fuels, such as air, hydrogen, or helium (with hydrogen the best and air the worst). Typical total efficiencies vs. high pressure/liter density

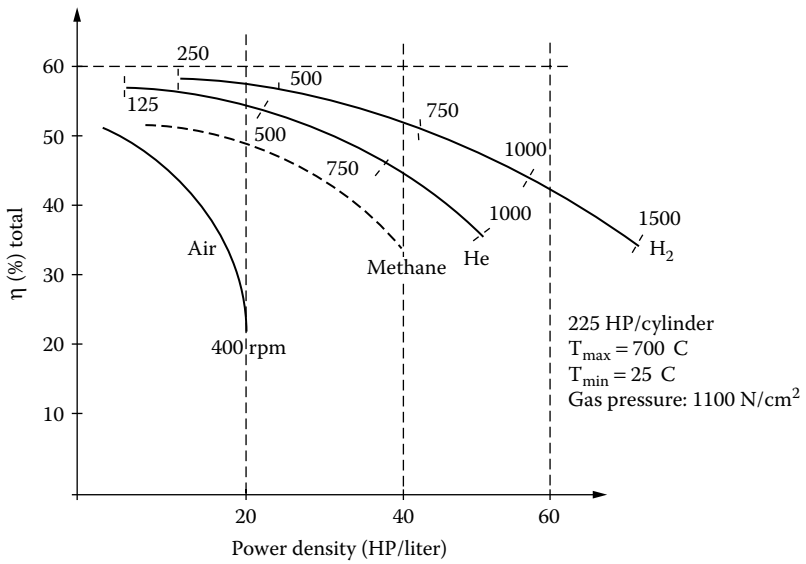

FIGURE 3.28 Efficiency/power density of Stirling engines.

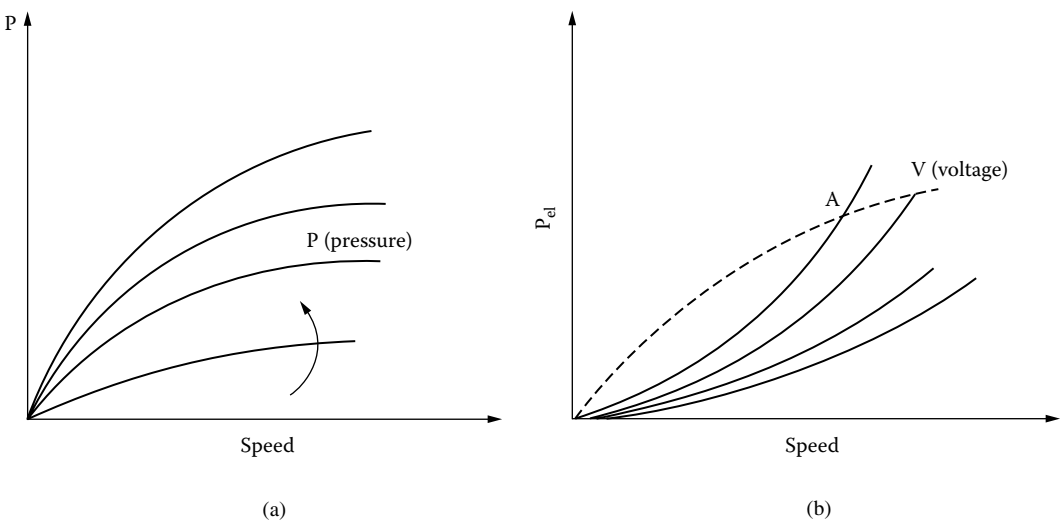

FIGURE 3.29 Power/speed curves: (a) the Stirling engine and (b) the electric generator.

are shown in Figure 3.28 [14] for three working fluids at various speeds. As the power and speed go up, the power density decreases. Methane may be a good replacement for air for better performance.

Typical power/speed curves of Stirling engines with pressure p are shown in Figure 3.29a. And, the power/speed curves of a potential electric generator, with speed, and voltage V as a parameter, appear in Figure 3.29b. The intersection at point A of the Stirling engine and the electric generator power/speed curves looks clearly like a stable steady-state operation point. There are many variants for rotary-motion Stirling engines [14].

3.7.3 Free-Piston Stirling Engines Modeling

Free-piston linear-motion Stirling engines were recently developed (by Sunpower and STC companies) for linear generators for spacecraft or home electricity production (Figure 3.30) [15].

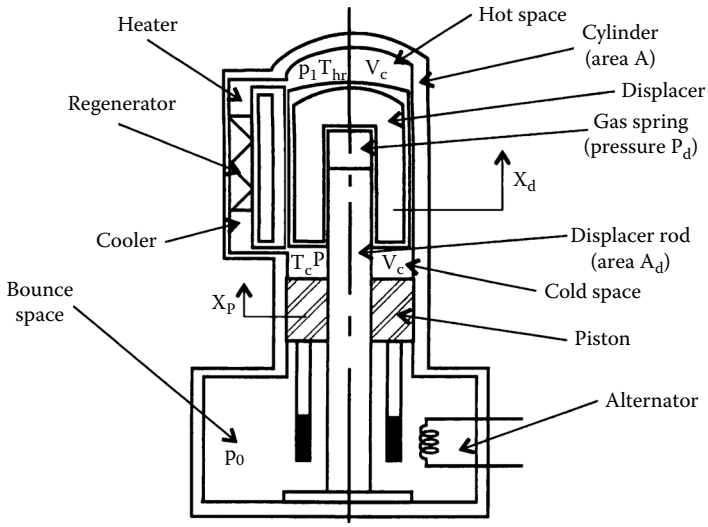

FIGURE 3.30 Linear Stirling engine with free-piston displacer mover.

The dynamic equations of the Stirling engine (Figure 3.30) are as follows:

$$M_d \overset{\infty\infty}{X}_d + D_d \overset{\infty}{X}_d = A_d(P_p - P) \tag{3.22}$$

for the normal displacer, and

$$M_p \overset{\infty\infty}{X}_p + D_p \overset{\infty}{X}_p + F_{elm} + K_p X_p + \left(A - A_d\right)\frac{\partial P}{\partial x_d} X_d = 0 \tag{3.23}$$

for the piston, where

A_d = the displacer rod area (m^2)
D_d = the displacer damping constant (N/msec)
P_d = the gas spring pressure (N/m^2)
P = the working gas pressure (N/m^2)
D_p = the piston damping constant (N/msec)
X_d = the displacer position (m)
X_p = the power piston position (m)
A = the cylinder area (m^2)
M_d = the displacer mass (kg)
M_p = the power piston mass (kg)
F_{elm} = the electromagnetic force (of linear electric generator) (N)

Equation 3.22 through Equation 3.23 may be linearized as follows:

$$\begin{aligned} M_d \overset{\infty\infty}{X}_d + D_d \overset{\infty}{X}_d &= -K_d X_d - \alpha_p X_p \\ M_p \overset{\infty\infty}{X}_p + D_p \overset{\infty}{X}_p + F_{elm} &= -K_p X_p - \alpha_T X_d \end{aligned} \tag{3.24}$$

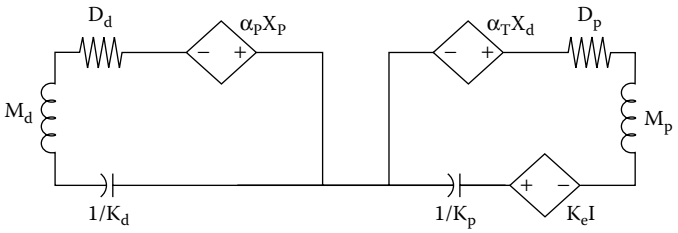

FIGURE 3.31 Free-piston Stirling engine dynamics model.

$$K_d = -A_d \frac{\partial P_d}{\partial X_d} - \frac{\partial P}{\partial X_d}; \alpha_p = \frac{\partial P}{\partial X_d} A_d$$
$$K_p = \left(A - A_d\right) \frac{\partial P}{\partial X_p}; \alpha_T = \left(A - A_d\right) \frac{\partial P}{\partial X_d}; F_{elm} = K_e I \tag{3.25}$$

where I is the generator current.

The electric circuit correspondent of Equation 3.25 is shown in Figure 3.31.

The free-piston Stirling engine model in Equation 3.25 is a fourth-order system, with $X_d, \overset{\infty}{X}_d, X_p, \overset{\infty}{X}_p$ as variables. Its stability when driving a linear permanent magnet (PM) generator will be discussed in Chapter 12 of *Variable Speed Generators*, dedicated to linear reciprocating electric generators. It suffices to say here that at least in the kilowatt range, such a combination was proven stable in stand-alone or power-grid-connected electric generator operation modes.

The merits and demerits of Stirling engines are as follows:

- Independent from heat source: fossil fuels, solar energy
- Very quiet
- High theoretical efficiency; not so large in practice yet, but still 35 to 40% for $T_{max} = 800$ C and $T_{min} = 40$ C
- Reduced emissions of noxious gases
- High initial costs
- Conduction and storage of heat are difficult to combine in the regenerator
- Materials have to be heat resistant
- Heat exchanger is needed for the cooler for high efficiency
- Not easy to stabilize

A general qualitative comparison of thermal engines is summarized in Table 3.2.

3.8 Hydraulic Turbines

Hydraulic turbines convert the water energy of rivers into mechanical work at the turbine shaft. River water energy and tidal (wave) sea energy are renewable. They are the results of water circuits and are gravitational (tide energy) in nature, respectively. Hydraulic turbines are one of the oldest prime movers used by man.

The energy agent and working fluid is water, in general, the kinetic energy of water (Figure 3.32). Wind turbines are similar, but the wind/air kinetic energy replaces the water kinetic energy. Wind turbines will be treated separately, however, due to their many particularities. Hydraulic turbines are, generally, only prime movers, that is, motors. There are also reversible hydraulic machines that may operate either as turbines or as pumps. They are also called hydraulic turbine pumps. There are hydrodynamic transmissions made of two or more conveniently mounted hydraulic machines in a single frame. They play

TABLE 3.2

Parameter Thermal Engine	Combustion Type	Efficiency	Quietness	Emissions	Fuel Type	Starting	Dynamic Response
Steam turbines	Continuous	Poor	Not so good	Low	Multifuel	Slow	Slow
Gas turbines	Continuous	Good at full loads, low at low load	Good	Reduced	Independent	Easy	Poor
Stirling engines	Continuous	High in theory, lower so far	Very good	Very low	Independent	N/A	Good
Spark-ignition engines	Discontinuous	Moderate	Rather bad	Still large	One type	Fast	Very good
Diesel engines	Discontinuous	Good	Bad	Larger	One type	Rather fast	Good

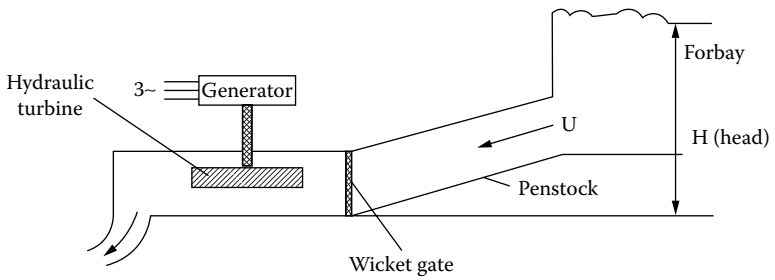

FIGURE 3.32 Hydropower plant schematics.

TABLE 3.3 Hydraulic Turbines

Turbine	Type	Head	Inventor	Trajectory
Tangential	Impulse	>300 m	Pelton (P)	Designed in the transverse plane
Radial-axial	Reaction	<50 m	Francis (F)	Bent into the axial plane
Axial	Reaction (propeller)	<50 m	Kaplan (K), Strafflo (S), Bulb (B)	Bent into the axial plane

the role of mechanical transmissions but have active control. Hydrodynamic transmissions fall beyond our scope here.

There are two main types of hydraulic turbines: impulse turbines for heads above 300 to 400 m, and reaction turbines for heads below 300 m. A more detailed classification is related to the main direction of the water particles in the rotor zone: bent axially or transverse to the rotor axis or related to the inventor (Table 3.3). In impulse turbines, the run is at atmospheric pressure, and all pressure drops occur in the nozzles, where potential energy is turned into kinetic energy of water which hits the runner. In reaction turbines, the pressure in the turbine is above the atmospheric pressure; water supplies energy in both potential and kinetic forms to the runner.

3.8.1 Hydraulic Turbines Basics

The terminology in hydraulic turbines is related to variables and characteristics [16]. The main variables are of geometrical and functional types:

- Rotor diameter: D_r (m)
- General sizes of the turbine

- Turbine gross head: H_T (m)
- Specific energy: $Y_T = gH_T$ (J/kg)
- Turbine input flow rate: Q (m³/sec)
- Turbine shaft torque: T_T (Nm)
- Turbine shaft power: P_T (W [kW, MW])
- Rotor speed: Ω_T (rad/sec)
- Liquid (rotor properties):
  - Density: ρ (kg/m³)
  - Cinematic viscosity: ν (m²/sec)
  - Temperature: T (C)
  - Elasticity module: E (N/m²)

The main characteristics of a hydraulic turbine are generally as follows:

- Efficiency:

$$\eta_T = \frac{P_T}{P_h} = \frac{T_T \cdot \Omega_r}{\rho g H_T Q} \tag{3.26}$$

- Specific speed n_S:

$$n_S = n\frac{\sqrt{P_T \cdot 0.736}}{H_T^{5/4}}, rpm \tag{3.27}$$

  with n equal to rotor speed in revolutions per minute, P_T is measured in kilowatts, and H_T in meters. The specific speed corresponds to a turbine that for a head of 1 m produces 1 HP (0.736 kW).
- Characteristic speed n_C:

$$n_c = \frac{n\sqrt{Q}}{H_T^{3/4}}, rpm \tag{3.28}$$

  n equals the rotor speed in revolutions per minute, Q equals the flow rate in cubic meters per second, and H_T is measured in meters.
- Reaction rate γ:

$$\gamma = \frac{p_1 - p_2}{\rho g H_T} \tag{3.29}$$

  where p_1, p_2 are the water pressures right before and after the turbine rotor. $\gamma = 0$ for Pelton turbines; ($p_1 = p_2$) for zero-reaction (impulse) turbines; and $0 < \gamma < 1$ for radial–axial and axial turbines (Francis, Kaplan turbines).
- Cavitation coefficient σ_T:

$$\sigma_T = \frac{\Delta h_i}{H_T} \tag{3.30}$$

  with Δh_i equal to the net positive suction head.

  It is good for σ_t to be small, $\sigma_t = 0.01 - 0.1$. It increases with n_S and decreases with H_T.

- Specific weight G_{sp}:

$$G_{sp} = \frac{G_T}{P_T}, N/kW \tag{3.31}$$

with G_T equal to the turbine mass × g, in N.
In general $G_{sp} \approx 70 - 150$ N/kW.

Generally, the rotor diameter $D_r = 0.2 - 12$ m, the head $H_T = 2 - 2000$ m, the efficiency at full load is $\eta_T = 0.8 - 0.96$, the flow rate $Q = 10^{-3} - 10^3$ m^3/sec, and rotor speed is $n \approx 50 - 1000$ rpm.

Typical variations of efficiency [16] with load are given in Figure 3.33. The maximum efficiency [16] depends on the specific speed n_S and on the type of turbine (Figure 3.34).

The specific speed is a good indicator of the best type of turbine for a specific hydraulic site. In general, $n_{Sopt} = 2 - 64$ for Pelton turbines, $n_S = 50 - 500$ for Francis turbines, and $n_S = 400 - 1700$ for Kaplan turbines. The specific speed n_S could be changed by changing the rotor speed n, the total power division in multiple turbines rotors or injectors, and the turbine head. The tendency is to increase n_S in order to reduce turbine size, by increasing rotor speed, at the costs of higher cavitation risk.

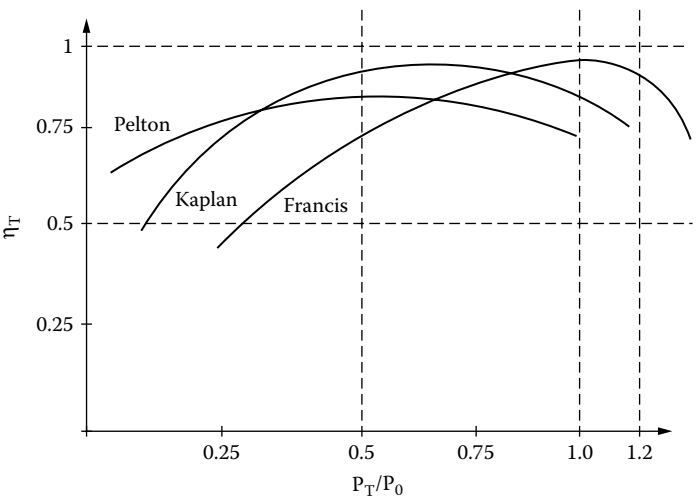

FIGURE 3.33 Typical efficiency/load for Pelton, Kaplan, and Francis turbines.

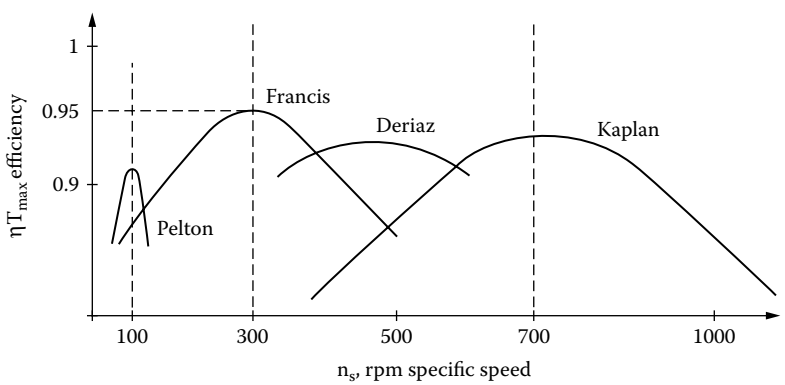

FIGURE 3.34 Maximum efficiency vs. specific speed.

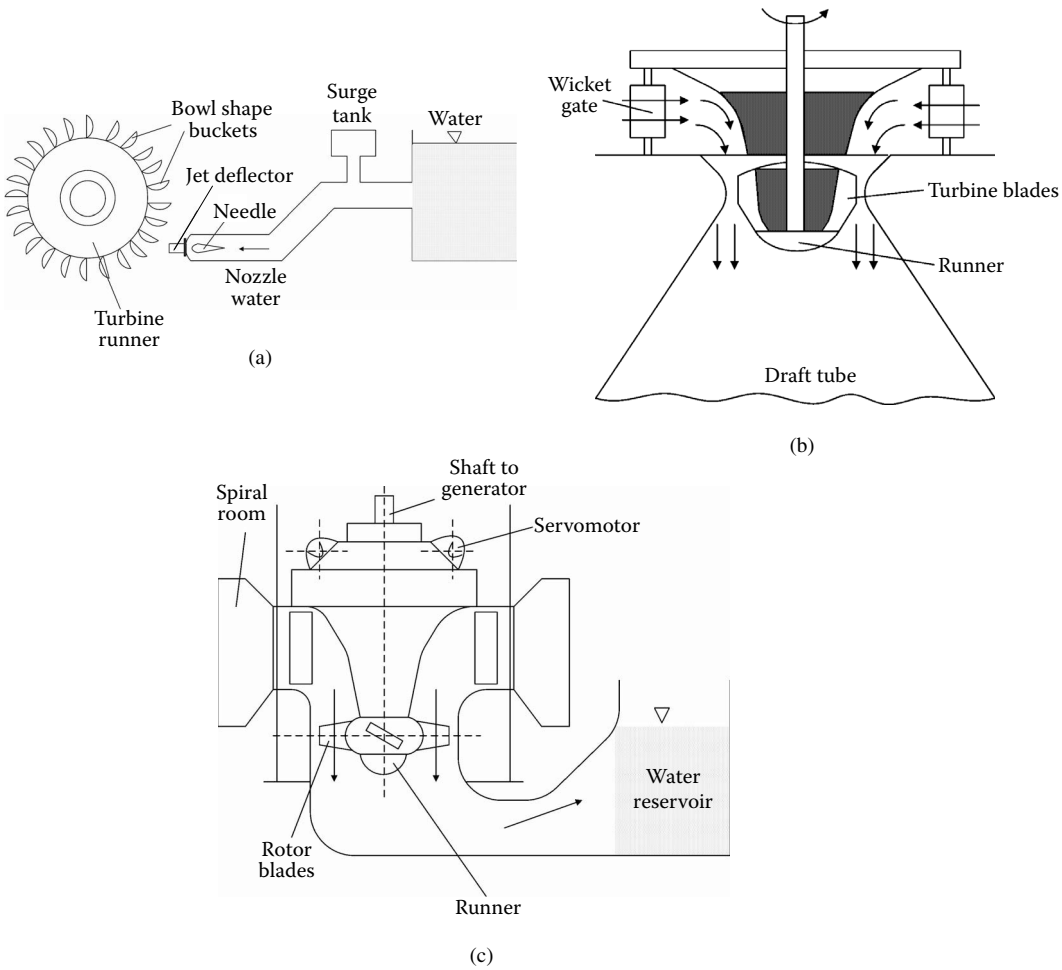

FIGURE 3.35 Hydraulic turbine topology: (a) Pelton type, (b) Francis type, and (c) Kaplan type.

As expected, the efficiency of all hydraulic turbines tends to be high at rated load. At part load, Pelton turbines show better efficiency. The worst at part load is the Francis turbine. It is, thus, the one more suitable for variable speed operation. Basic topologies for Pelton, Francis, and Kaplan turbines are shown in Figure 3.35a through Figure 3.35c.

In the high-head impulse (Pelton) turbine, the high-pressure water is converted into high-velocity water jets by a set of fixed nozzles. The high-speed water jets hit the bowl-shaped buckets placed around the turbine runner, and mechanical torque is produced at the turbine shaft. The area of the jet is controlled by a needle placed in the center of the nozzle. The needle is actuated by the turbine governor (servomotor). In the event of sudden load reduction, the water jet is deflected from the buckets by a jet deflector (Figure 3.35a).

In contrast, reaction (radial–axial) or Francis hydraulic turbines (Figure 3.35b) use lower head and high volumes of water, and run at lower speeds. The water enters the turbine from the intake passage or penstock, goes through a spiral chamber, then passes through the movable wicket gates onto the turbine runner, and then, through the draft tube, goes to the tail water reservoir. The wicket gates have their axes parallel to the turbine axis. In Francis turbines, the upper ends of the rotor blades are tightened to a crown and the lower ends to a band.

At even lower head, in Kaplan hydraulic turbines, the rotor blades are adjustable through an oil servomotor placed within the main turbine shaft.

3.8.2 A First-Order Ideal Model of Hydraulic Turbines

Usually, in system stability studies, with the turbine coupled to an electrical generator connected to a power grid, a simplified (classical) model of the hydraulic turbine is used. Such a model assumes that water is incompressible, the penstock is inelastic, the turbine power is proportional to the product of head and volume flow (volume flow rate), and the velocity of water varies with the gate opening and with the square root of net head [2].

There are three fundamental equations to consider:

- Water velocity u equation in the penstock
- Turbine shaft (mechanical) power equation
- Acceleration of water volume equation

According to the above assumptions, the water velocity in the penstock u is

$$u = K_u G\sqrt{H} \tag{3.32}$$

where

G = the gate opening
H = the net head at the gate

Linearizing this equation and normalizing it to rated quantities ($u_0 = K_u G_0 \sqrt{H_0}$) yields the following:

$$\frac{\Delta U}{U_0} = \frac{\Delta H}{2H_0} + \frac{\Delta G}{G_0} \tag{3.33}$$

The turbine mechanical power P_m is written

$$P_m = K_p HU \tag{3.34}$$

After normalization ($P_{m0} = K_p H_0 U_0$) and linearization, Equation 3.34 becomes

$$\frac{\Delta P_m}{P_0} = \frac{\Delta H}{H_0} + \frac{\Delta U}{U_0} \tag{3.35}$$

Substituting $\frac{\Delta H}{H_0}$ or $\frac{\Delta U}{U_0}$ from Equation 3.33 into Equation 3.35 yields the following:

$$\frac{\Delta P_m}{P_0} = 1.5\frac{\Delta H}{H_0} + \frac{\Delta G}{G_0} \tag{3.36}$$

and finally,

$$\frac{\Delta P_m}{P_0} = 3\frac{\Delta U}{U_0} - 2\frac{\Delta G}{G_0} \tag{3.37}$$

The water column that accelerates due to change in head at the turbine is described by its motion equation:

$$\rho LA\frac{d\Delta U}{dt} = -A(\rho g)\Delta H \tag{3.38}$$

where

ρ = the mass density
L = the conduit length
A = the pipe area
g = the acceleration of gravity

By normalization, Equation 3.38 becomes

$$T_W \frac{d}{dt}\frac{\Delta U}{U_0} = -\frac{\Delta H}{H_0} \tag{3.39}$$

where

$$T_W = \frac{LU_0}{gH_0} \tag{3.40}$$

is the water starting time. It depends on load, and it is in the order of 0.5 sec to 5 sec for full load.

Replacing d/dt with the Laplace operator, from Equation 3.33 and Equation 3.39, one obtains the following:

$$\frac{\dfrac{\Delta U}{U_0}}{\dfrac{\Delta G}{G_0}} = \frac{1}{1+\dfrac{T_W}{2}s} \tag{3.41}$$

$$\frac{\dfrac{\Delta P_m}{P_0}}{\dfrac{\Delta G}{G_0}} = \frac{1-T_W \cdot s}{1+\dfrac{T_W}{2}s} \tag{3.42}$$

The transfer functions in Equation 3.41 and Equation 3.42 are shown in Figure 3.36. The power/gate opening transfer function (Equation 3.42) has a zero in the right s plane. It is a nonminimum phase system that cannot be identified completely by investigating only its amplitude from its amplitude/frequency curve.

For a step change in gate opening, the initial and final value theorems yield the following:

$$\frac{\Delta P_m}{P_0}(0) = \lim_{s\to\infty} s\frac{1}{s}\frac{1-T_w s}{1+\dfrac{1}{2}T_w s} = -2 \tag{3.43}$$

$$\frac{\Delta P_m}{P_0}(\infty) = \lim_{s\to 0}\frac{1-T_w s}{1+\dfrac{1}{2}T_w s} = 1.0 \tag{3.44}$$

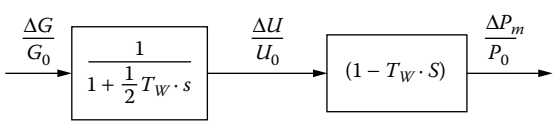

FIGURE 3.36 The linear ideal model of hydraulic turbines in P.U..

The time response to such a gate step opening is

$$\frac{\Delta P_m}{P_0}(t) = \left(1 - 3e^{-2t/T_W}\right)\frac{\Delta G}{G_0} \tag{3.45}$$

After a unit step increase in gate opening, the mechanical power goes first to a –2 P.U. value and only then increases exponentially to the expected steady state value of 1 P.U. This is due to water inertia.

Practice has shown that this first-order model hardly suffices when the perturbation frequency is higher than 0.5 rad/sec. The answer is to investigate the case of the elastic conduit (penstock) and compressible water where the conduit of the wall stretches at the water wave front.

3.8.3 Second- and Higher-Order Models of Hydraulic Turbines

We start with a slightly more general small deviation (linear) model of the hydraulic turbine [17]:

$$\begin{aligned} q &= a_{11}h + a_{12}n + a_{13}z \\ m_t &= a_{21}h + a_{22}n + a_{23}z \end{aligned} \tag{3.46}$$

where

q = the volume flow
h = the net head
n = the turbine speed
z = the gate opening m_t – shaft torque

All variables are measured in P.U. values. As expected, the coefficients a_{11}, a_{12}, a_{13}, a_{21}, a_{22}, a_{23} vary with load and other changes. To a first approximation, $a_{12} \approx a_{22} \approx 0$, and, with constant a_{ij} coefficients, the first-order model is reclaimed.

Now, if the conduit is considered elastic and water as compressible, the wave equation in the conduit may be modeled as an electric transmission line that is open circuited at the turbine end and short-circuited at forebay.

Finally, the incremental head and volume flow rate $h(s)/q(s)$ transfer function of the turbine is as follows [2]:

$$\frac{h(s)}{q(s)} = -\frac{T_w}{T_e}\tanh(Te \cdot s + F) \tag{3.47}$$

where

F = the friction factor
T_e = the elastic time constant of the conduit

$$T_e = \frac{conduit\_length : L}{wave\_velocity : a}; a = \sqrt{g/\alpha} \tag{3.48}$$

$$\alpha = \rho g\left(\frac{1}{K} + \frac{D}{Ef}\right) \tag{3.49}$$

where

ρ = the water density
g = the acceleration of gravity

f = the thickness of the conduit wall
D = the conduit diameter
K = the bulk modulus of water compression
E = the Young's modulus of elasticity for the pipe material

Typical values of a are around 1200 m/sec for steel conduits and around 1400 m/sec for rock tunnels. T_e is in the order of fractions of a second and is larger for larger penstocks (Pelton turbines).

If we now introduce Equation 3.41 and Equation 3.42 in Equation 3.47, the power $\Delta P_m(s)$ to gate opening $\Delta z(s)$ in P.U. transfer functions is obtained:

$$G(s) = \frac{\Delta P_m}{\Delta z}(s) = \frac{1 - \frac{T_W}{T_e}\tanh\left(T_e \cdot s + F\right)}{1 + \frac{T_W}{2T_e}\tanh\left(T_e \cdot s + F\right)} \tag{3.50}$$

Alternatively, from Equation 3.46,

$$G'(s) = \frac{\Delta P_m}{\Delta z}(s) = \frac{1 - q_p - \frac{T_W}{T_e}\tanh\left(T_e \cdot s + F\right)}{1 + 0.5q_p + \frac{T_W}{2T_e}\tanh\left(T_e \cdot s + F\right)} \tag{3.51}$$

where q_p accounts for friction.

With $F = q_p = 0$, Equation 3.50 and Equation 3.51 degenerate into the first-order model provided tan$h$ $T_{es} \approx T_{es}$, that is, for very low frequencies:

$$G_1(s) = \frac{1 - T_W \cdot s}{1 + \frac{T_W}{2} \cdot s} \tag{3.52}$$

The frequency response ($s = j\omega$) of Equation 3.50 with $F = 0$ is shown in Figure 3.37.

Now, we may approximate the hyperbolic function with truncated Taylor series [18]:

$$\begin{aligned} \tanh(T_e \cdot s) &= \frac{T_e \cdot s}{1 + \left(\frac{T_e \cdot s}{2}\right)^2} \\ G_2(s) &= \frac{\left(T_e \cdot s\right)^2 - 2T_W \cdot s + 2}{\left(T_e \cdot s\right)^2 + T_W \cdot s + 2} \end{aligned} \tag{3.53}$$

Figure 3.37 shows comparative results for $G(s)$, $G_1(s)$, and $G_2(s)$ for $T_e = 0.25$ sec and $T_w = 1$ sec.

The second-order transfer function (Figure 3.38) performs quite well to and slightly beyond the first maximum, which occurs in our case at

$$\omega = \frac{\pi}{2T_e} = 6.28 \text{ rad/sec}$$

It is, however, clear that well beyond this frequency, a higher-order approximation is required.

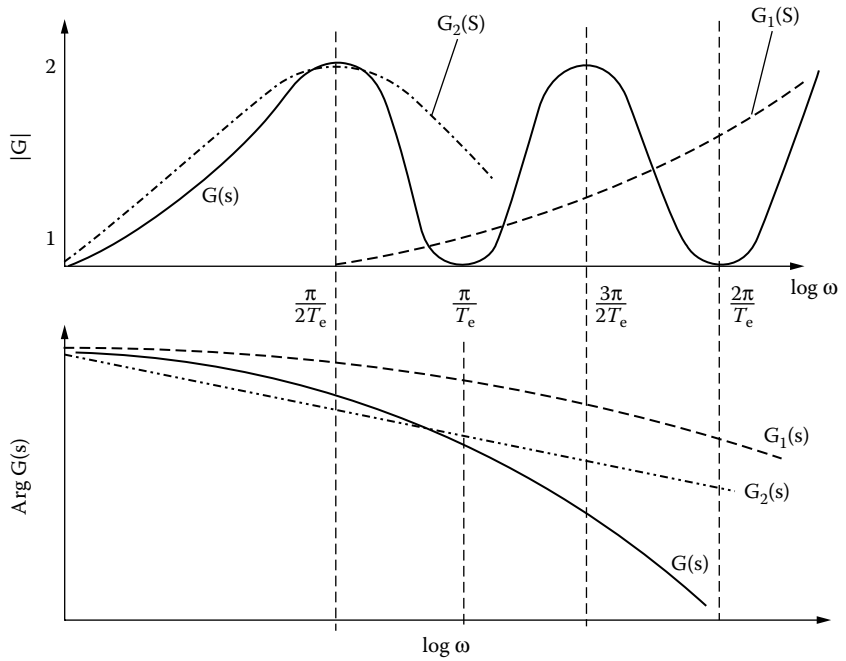

FIGURE 3.37 Higher-order hydraulic turbine frequency response.

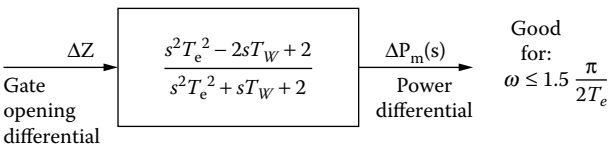

FIGURE 3.38 The second-order model of hydraulic turbines (with zero friction).

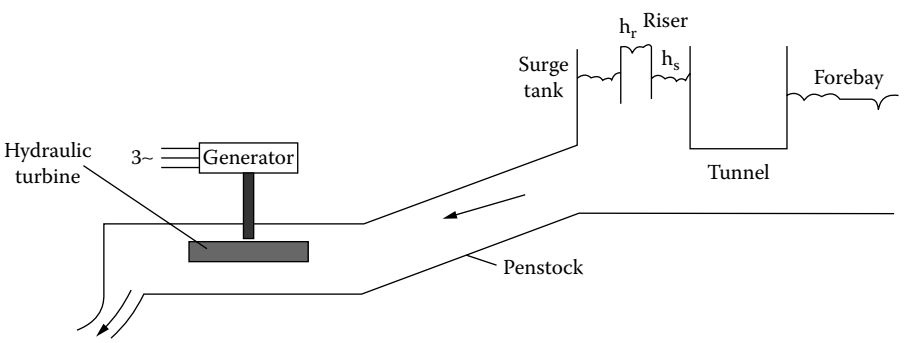

FIGURE 3.39 Hydraulic plant with surge tank.

Such models can be obtained with advanced curve-fitting methods applied to $G_2(s)$ for the frequency range of interest [19,20].

The presence of a surge tank (Figure 3.39) in some hydraulic plants calls for a higher-order model.

The wave (transmission) line equations apply now both for tunnel and penstock. Finally, the tunnel and surge tank can be approximated to $F_1(s)$ [2]:

$$F_1(s) = \frac{q_c + s \cdot T_{WC}}{1 + s \cdot T_s \cdot q_c + s^2 T_{WC} T_S} = -\frac{h_S}{U_p}$$

$$\tanh\left(T_{ec} \cdot s\right) = T_{ec} \cdot s \tag{3.54}$$

$$Z_c = \frac{T_{WC}}{T_{ec}}$$

where

T_{ec} = the elastic time constant of the tunnel
T_{WC} = the water starting time in the tunnel
q_c = the surge tank friction coefficient
h_S = the surge tank head
U_p = the upper penstock water speed
T_S = the surge tank riser time ($T_S \approx 600 - 900$ sec)

Now for the penstock, the wave equation yields (in P.U.) the following:

$$h_t = h_r \sec h(T_{ep} \cdot s) - Z_p U_t \tanh(T_{ep} \cdot s) - q_p U_t$$

$$U_p = U_t \cosh\left(T_{ep} \cdot s\right) + \frac{h_t}{Z_p} \sinh\left(T_{ep} \cdot s\right) \tag{3.55}$$

where

Z_p = the hydraulic impedance of the penstock $\left(Z_p = \frac{T_{Wp}}{T_{ep}}\right)$

q_p = the friction coefficient in the penstock
T_{ep} = the penstock elastic time
T_{Wp} = the penstock water starting time
h_r = the riser head
h_t = the turbine head

The overall water velocity U_p to head at turbine h_t ratio is as follows [2]:

$$F(s) = \frac{U_p}{h_t} = -\frac{\left(1 + F_1(s) \times \tanh\left(T_{ep} \cdot s\right) / Z_p\right)}{q_p + F_1(s) + Z_p \tanh\left(T_{ep} \cdot s\right)} \tag{3.56}$$

The power differential is written

$$P_m = U_t h_t \text{ in P.U.} \tag{3.57}$$

$F(s)$ now represents the hydraulic turbine with wave (hammer) and surge tank effects considered.

If we add Equation 3.32, which ties the speed at turbine head and gate opening to Equation 3.56 and Equation 3.57, the complete nonlinear model of the hydraulic turbine with penstock and surge tank effects included (Figure 3.40) is obtained.

Notice that g_{fL} and g_{NL} are the full-load and no-load actual gate openings in P.U.

Also, h_0 is the normalized turbine head, U_0 is the normalized water speed at the turbine, U_{NL} is the no-load water speed at the turbine, ω_r is the shaft speed, P_m is the shaft power, and m_t is the shaft torque differential in P.U. values.

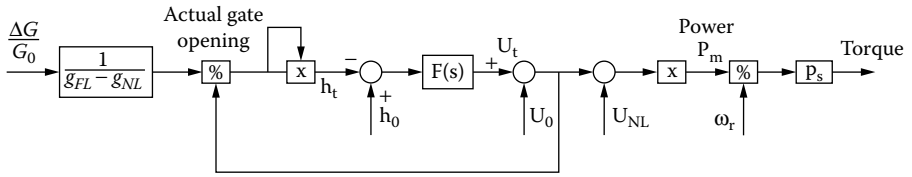

FIGURE 3.40 Nonlinear model of hydraulic turbine with hammer and surge tank effects.

The nonlinear model in Figure 3.40 may be reduced to a high-order (three or more) linear model through various curve fittings applied to the theoretical model with given parameters. Alternatively, frequency response tests may be fitted to a third-order, fourth-order, and so forth, linear system for preferred frequency bands [21].

As the nonlinear complete model is rather involved, the question arises as to when it should be used. Fortunately, only in long-term dynamic studies is it mandatory.

For governor timing studies, as the surge tank natural period (T_s) is of the order of minutes, its consideration is not necessary. Further on, the hammer effect should be considered, but the second-order model suffices.

In transient stability studies, again, the hammer effect should be considered.

For small-signal stability studies, linearization of the turbine penstock model (second-order model) may also be adequate, especially in plants with long penstocks.

3.8.4 Hydraulic Turbine Governors

In principle, hydraulic turbine governors are similar to those used for steam and gas turbines. They are mechanohydraulic or electrohydraulic. In general, for large power levels, they have two stages: a pilot valve servomotor and a larger power gate-servomotor. A classical system with speed control and good performance is shown in Figure 3.41.

T_{PV} = the pilot valve with servomotor time constant (0.05 sec)
T_{GV} = the main (gate) servomotor time constant (0.2 sec)
K_V = the servo (total) gain (5)
$R_{max\ open}$ = the maximum gate opening rate ≈ 0.15 P.U./sec
$R_{max\ close}$ = the maximum closing rate ≈ 0.15 P.U./sec
T_R = the reset time (5 sec)
R_P = the permanent drop (0.04)
R_T = the transient drop (0.4)

Numbers in parentheses above are sample data [2] given only to get a feeling for magnitudes.

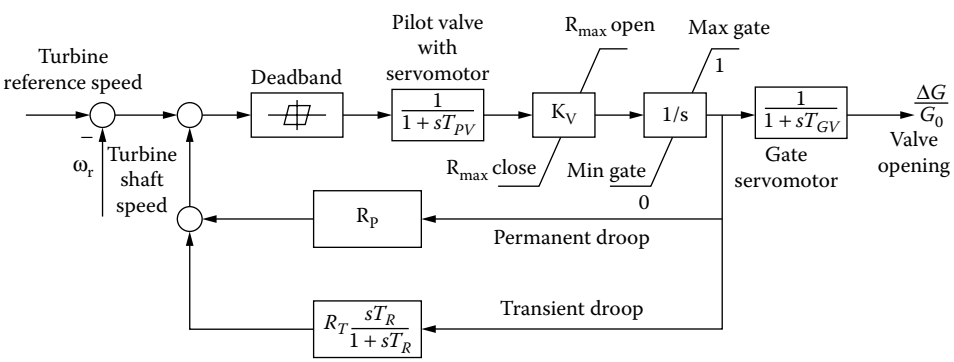

FIGURE 3.41 Typical (classical) governor for hydraulic turbines.

A few remarks on the model in Figure 3.41 are in order:

- The pilot–valve servomotor (lower power stage of governor) may be mechanical or electric; electric servomotors tend to provide faster and more controllable responses.
- Water is not very compressible; thus, the gate motion has to be gradual; near the full closure, even slower motion is required.
- Deadband effects are considered in Figure 3.41, but their identification is not an easy task.
- Stable operation during system islanding (stand-alone operation mode of the turbine–generator system) and acceptable response quickness and robustness under load variations are the main requirements that determine the governor settings.
- The presence of a transient compensation drop is mandatory for stable operation.
- For islanding operation, the choice of temporary drop R_T and reset time T_R is essential; they are related to water starting time constant T_W and mechanical (inertia) time constant of the turbine–generator set T_M. Also, the gain K_V should be high.
  - According to Reference [2],

$$
\begin{aligned}
R_T &= \left[2.3 - \left(T_W - 1.0\right)0.15\right]\frac{T_W}{T_M} \\
T_R &= \left[5.0 - \left(T_W - 1.0\right)0.5\right]T_W \\
T_M &= 2H; \\
H &= \frac{J\omega_0^2}{2S_0}(s)
\end{aligned}
\tag{3.58}
$$

where

$J(\text{kgm}^2)$ = the turbine/generator inertia
ω_0 = the rated angular speed (rad/sec)
S_0 = the rated apparent power (VA) of the electrical generator

- In hydraulic turbines where wicket gates (Figure 3.41) are also used, the governor system has to control their motion also, basing its control on an optimization criterion.

The governing system becomes more involved. The availability of high-performance nonlinear motion controllers (adaptive, variable structure, fuzzy logic, or artificial neural networks) and of various powerful optimization methods [22] puts the governor system control into a new perspective (Figure 3.42).

Though most such advanced controllers have been tried on thermal prime movers and, especially, on power system stabilizers that usually serve only the electric generator excitation, the time for comprehensive digital online control of the whole turbine generator system seems ripe [23, 24]. Still, problems with safety could delay their aggressive deployment; not for a long time, though, we think.

3.8.5 Reversible Hydraulic Machines

Reversible hydraulic machines are, in fact, turbines that work part time as pumps, especially in pump-storage hydropower plants.

Pumping may be required either for land irrigation or for energy storage during off-peak electric energy consumption hours. It is also a safety and stability improvement vehicle in electric power systems in the presence of fast variations of loads over the hours of the day.

As up to 400 MW per unit pump-storage hydraulic turbine pumps are already in operation [25], their "industrial" deployment seems near. Pump-storage plants with synchronous (constant) speed generators (motors) are a well-established technology.

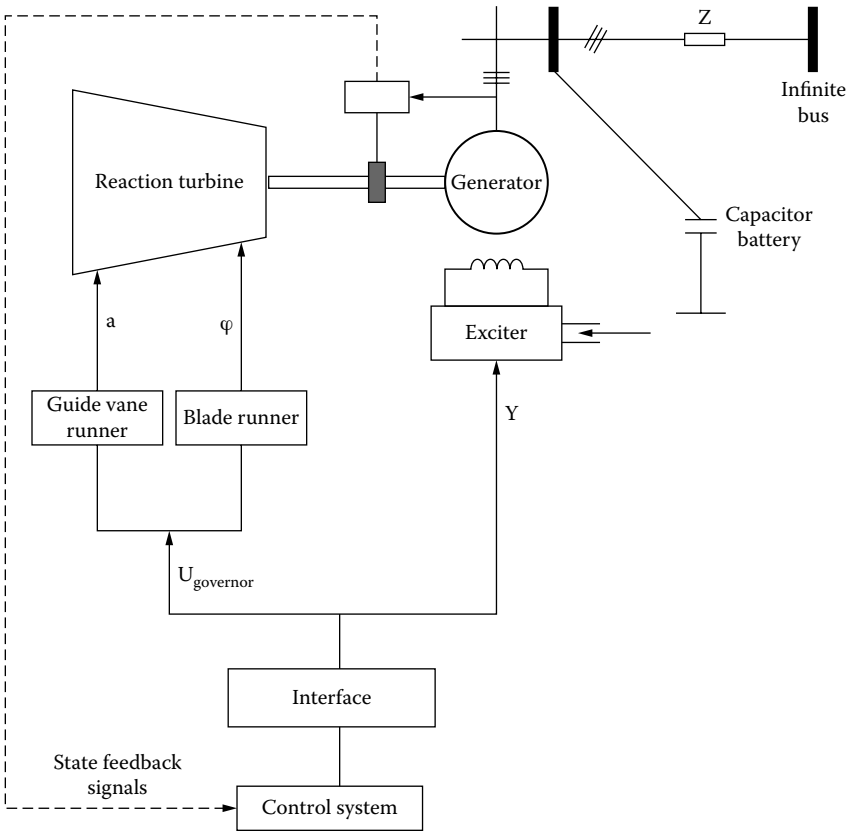

FIGURE 3.42 Coordinated turbine governor–generator–exciter–control system.

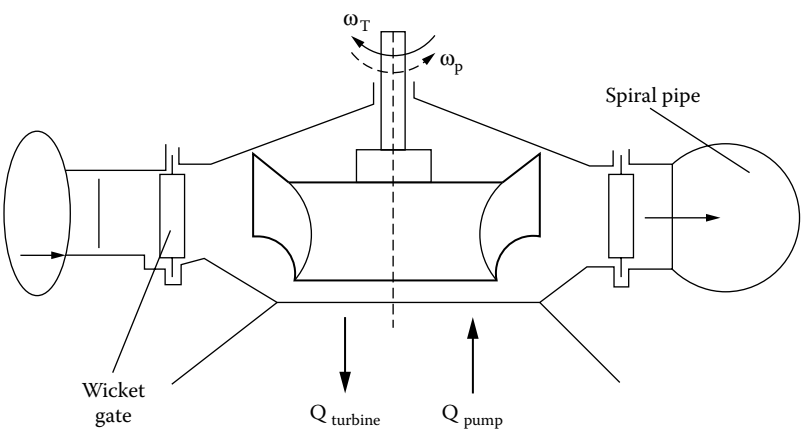

FIGURE 3.43 Radial–axial turbine pump with reversible speed.

A classification of turbine pumps is in order:

- By topology:
  - Radial–axial (Russel Dam) (Figure 3.43)
  - Axial (Annapolis) (Figure 3.44)

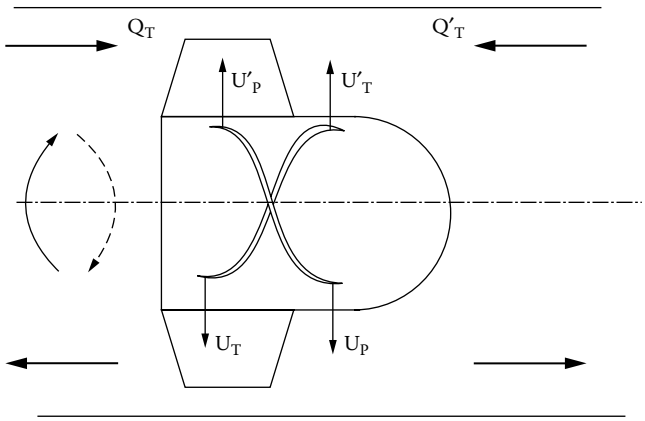

FIGURE 3.44 Axial turbine pump.

- By direction of motion:
  - With speed reversal for pumping (Figure 3.43 and Figure 3.44)
  - Without speed reversal for pumping
- By direction of fluid flow/operation mode:
  - Unidirectional/operation mode (Figure 3.43)
  - Bidirectional/operation mode (Figure 3.44)

There are many topological variations in existing turbine pumps; it is also feasible to design the machine for pumping and then check the performance for turbining, when the direction of motion is reversible.

With pumping and turbining in both directions of fluid flow, the axial turbine pump in Figure 3.44 may be adequate for tidal-wave power plants.

The passing from turbine to pump mode implies the emptying of the turbine chamber before the machine is started by the electric machine as the motor to prepare for pumping. This transition takes time.

More complicated topologies are required to secure unidirectional rotation for both pumping and turbining, though the time to switch from turbining to pumping mode is much shorter.

In order to preserve high efficiency in pumping, the speed in the pumping regime has to be larger than the one for turbining. In effect, the head is larger and the volume flow lower in pumping. A typical ratio for speed would be $\omega_p \approx (1.12 - 1.18)\ \omega_T$. Evidently, such a condition implies adjustable speed and power electronics control on the electric machine side. Typical head/volume flow characteristics [16] for a radial–axial turbine/pump are shown in Figure 3.45. They illustrate the fact that pumping is more efficient at higher speed than turbining and at higher heads, in general. Similar characteristics portray the output power vs. static head for various wicket gate openings [25] (Figure 3.46).

Power increases with speed and higher speeds are typical for pumping. Only wicket gate control by a governor system is used, as adjustable speed is practiced through instantaneous power control in the generator rotor windings, through power electronics.

The turbine governor and electric machine control schemes are specific for generating electric power (turbining) and for pumping [25].

In tidal-wave turbine/pumps, to produce electricity, a special kind of transit takes place from turbining to pumping in one direction of motion and in the other direction of motion in a single day. The static head changes from 0 to 100% and reverses sign (Figure 3.47). These large changes in head are expected to produce large electric power oscillations in the electric power delivered by the generator/motor driven by the turbine pump. Discontinuing operation between pumping and turbining and electric solutions based on energy storage are to be used to improve the quality of power delivered to the electrical power system.

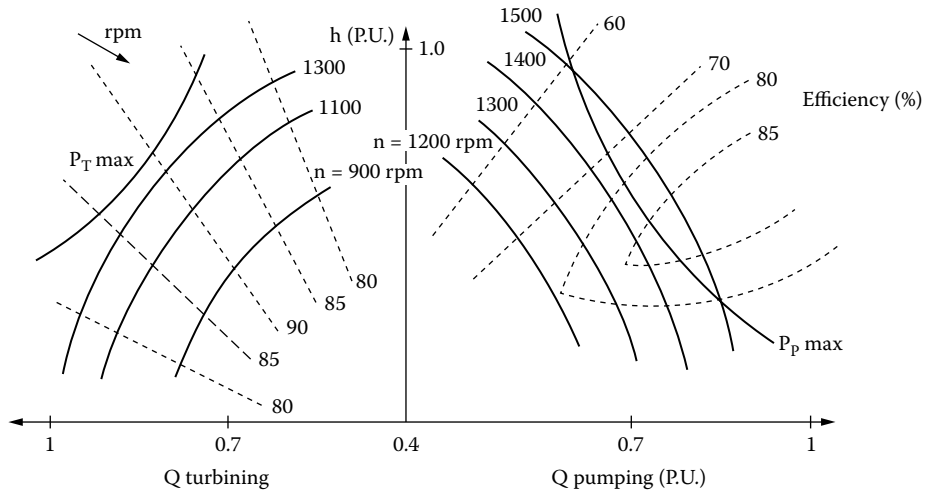

FIGURE 3.45 Typical characteristics of the pumping system of a radial–axial turbine plus pump.

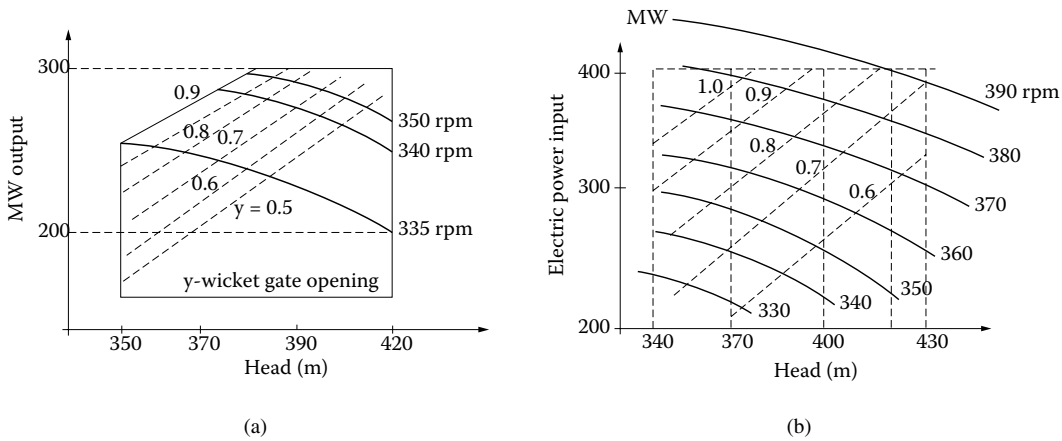

FIGURE 3.46 (a) Turbine/pump system and (b) power/static head curves at various speeds.

3.9 Wind Turbines

Air-pressure gradients along the surface of the Earth produce wind with direction and speed that are highly variable. Uniformity and strength of the wind are dependent on location, height above the ground, and size of local terrain irregularities. In general, wind airflows may be considered turbulent.

In a specific location, the variation of wind speed along the cardinal directions may be shown as in Figure 3.48a. This is important information, as it leads to the optimum directioning of the wind turbine, in the sense of extracting the largest energy from wind per year.

Wind speed increases with height (Figure 3.48b) and becomes more uniform. Designs with higher height/turbine diameter lead to more uniform flow and higher energy extraction. These designs come with the price of more expensive towers that are subject to increased structural vibrations.

With constant energy conversion, the turbine power increases approximately with cubic wind speed (u^3) up to a design limit, u_{max}. Above u_{max} (P_{rated}), the power of the turbine is kept constant by some turbine governor control to avoid structural or mechanical inadmissible overload (Figure 3.49).

For a given site, the wind is characterized by the so-called speed deviation (in P.U. per year). For example,

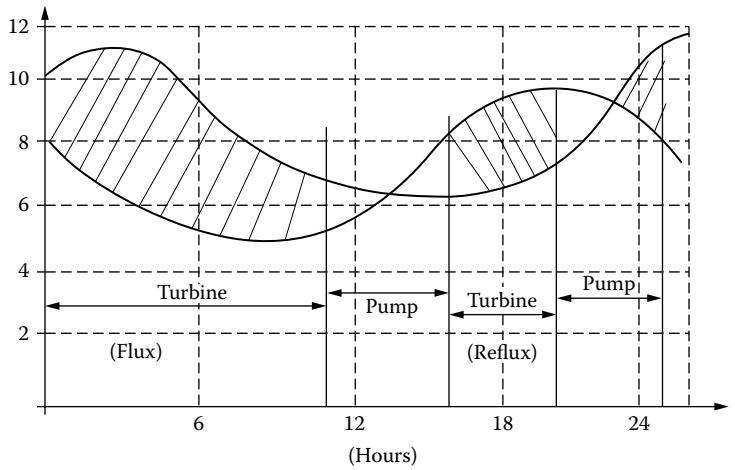

FIGURE 3.47 Head/time of the day in a tidal-wave turbine/pump.

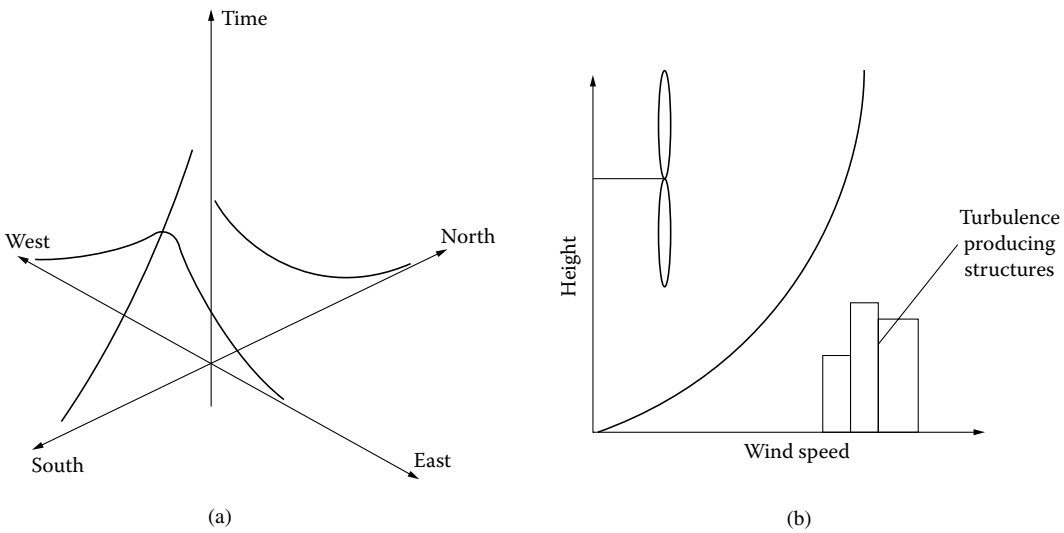

FIGURE 3.48 Wind speed vs. (a) location and (b) height.

$$\frac{t}{t_{\max}} = e^{-U^4} \tag{3.59}$$

The slope of this curve is called speed/frequency curve *f*:

$$f(U) = -\frac{d\left(\dfrac{t}{t_{\max}}\right)}{dU} \tag{3.60}$$

The speed/time is monotonical (as speed increases, its time occurrence decreases), but the speed/frequency curve generally experiences a maximum. The average speed U_{ave} is defined as follows:

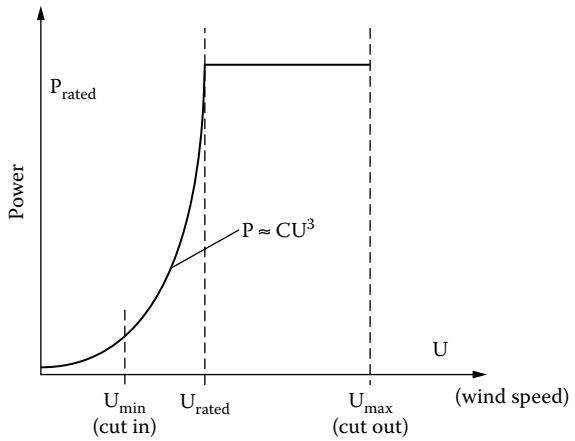

FIGURE 3.49 Wind turbine power vs. wind speed.

$$U_{ave} = \int_0^\infty Uf(U)dU \tag{3.61}$$

Other mean speed definitions are also used.

The energy content of the wind E, during t_{max} (1 year) is then obtained from the integral:

$$\frac{Energy\_during\_t_{max}}{\rho \cdot (disc\_area)} = \int_0^\infty U^3 f(U)dU \tag{3.62}$$

with $E(U) = U^3 f(U)$, the energy available at speed U. Figure 3.50 illustrates this line of thinking.

The time average speed falls below the frequency/speed maximum f_{max}, which, in turn, is smaller than the maximum energy per unit speed range E_{max}.

The adequate speed zone for efficient energy extraction is also apparent in Figure 3.50.

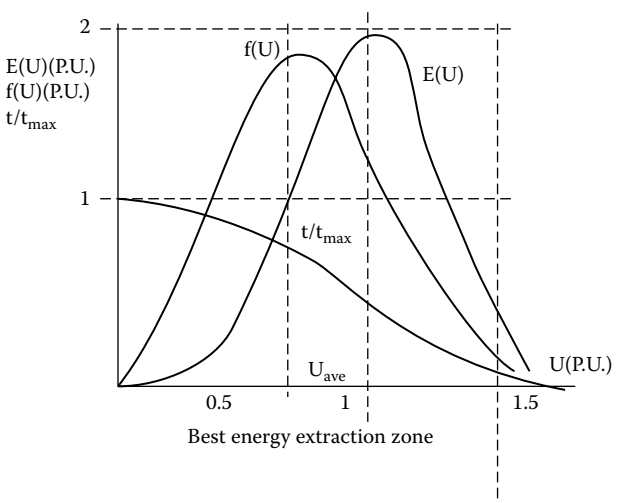

FIGURE 3.50 Sample time/speed, frequency/speed (f), and energy (E)/speed.

It should be borne in mind that these curves, or their approximations, depend heavily on location. In general, inland sites are characterized by large variations of speed over the day and month, while winds from the sea tend to have smaller variations in time.

Good extraction of energy over a rather large speed span, as in Figure 3.50, implies operation of the wind turbine over a pertinent speed range. The electric generator has to be capable of operating at variable speed in such locations.

There are constant-speed and variable-speed wind turbines.

3.9.1 Principles and Efficiency of Wind Turbines

For centuries, windmills operated in countries including Holland, Denmark, Greece, Portugal, and others. The best locations are situated either in the mountains or by the sea or by the ocean shore (or offshore). Wind turbines are characterized by the following:

- Mechanical power P(W)
- Shaft torque (Nm)
- Rotor speed n (rpm) or ω_r (rad/sec)
- Rated wind speed U_R
- Tip speed ratio:

$$\lambda = \frac{\omega_r \cdot D_r / 2}{U} = \frac{rotor\_blade\_tip\_speed}{wind\_speed} \tag{3.63}$$

The tip speed ratio $\lambda < 1$ for slow-speed wind turbines, and $\lambda > 1$ for high-speed wind turbines. The power efficiency coefficient C_p is as follows:

$$C_p = \frac{8P}{\rho\pi D_r^2 \cdot U^3} <> 1 \tag{3.64}$$

In general, C_p is a single maximum function of λ that strongly depends on the type of the turbine. A classification of wind turbines is thus in order:

- Axial (with horizontal shaft)
- Tangential (with vertical shaft)

The axial wind turbines may be slow (Figure 3.51a) and rapid (Figure 3.51b). The shape of the rotor blades and their number are quite different for the two configurations.

The slow axial wind turbines have a good starting torque and the optimum tip speed ratio $\lambda_{opt} \approx 1$, but their maximum power coefficient $C_{pmax}(\lambda_{opt})$ is moderate ($C_{pmax} \approx 0.3$). In contrast, rapid axial wind turbines self-start at higher speeds (above 5 m/sec wind speed), but for an optimum tip speed ratio $\lambda_{opt} \geq 7$, they have a maximum power coefficient $C_{pmax} \approx 0.4$, that is, a higher energy conversion ratio (efficiency).

For each location, the average wind speed U_{ave} is known. The design wind speed U_R is generally around 1.5 U_{ave}. The optimum tip speed ratio λ_{opt} increases as the number of rotor blades Z_1 decreases:

$$(\lambda_{opt}, Z_1) = (1, 8\text{–}24; 2, 6\text{–}12; 3, 3\text{–}6; 4, 2\text{–}4; 5, 2\text{–}3; >5, 2) \tag{3.65}$$

Three or two blades are typical for rapid axial wind turbines.

The rotor diameter D_r, may be, to a first approximation, calculated from Equation 3.64 for rated (design conditions) — P_{rated}, λ_{opt}, C_{popt}, U_R — with the turbine speed from Equation 3.63.

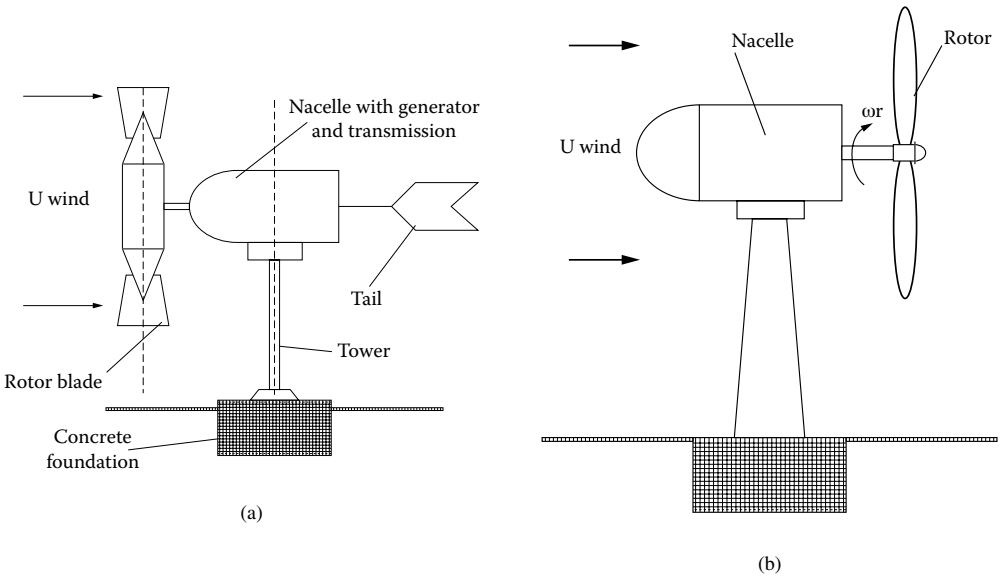

FIGURE 3.51 Axial wind turbines: (a) slow (multiblade) and (b) rapid (propeller).

Tangential (vertical shaft) wind turbines were built in quite a few configurations. They are of two subtypes: drag and lift. The axial (horizontal axis) wind turbines are all of the lift subtype. Some of the tangential wind turbine configurations are shown in Figure 3.52. While the drag subtype (Figure 3.52a) works at slow speeds ($\lambda_{opt} < 1$), the lift subtype (Figure 3.52b) works at high speeds ($\lambda_{opt} > 1$). Slow wind turbines have a higher self-starting torque but a lower power efficiency coefficient C_{pmax}. The efficiency limit (Betz limit) may be calculated by portraying the ideal wind speed and pressure profile before and after the turbine (Figure 3.53, [1]). The wind speed decreases immediately before and after the turbine disk plane, while a pressure differential also takes place. The continuity principle shows that

$$u_1 A_1 = u_\infty A_\infty \tag{3.66}$$

If the speed decreases along the direction of the wind speed, $u_1 > u_\infty$, and thus, $A_1 < A_\infty$.

The wind power P_{wind} in front of the wind turbine is the product of mass flow to speed squared per 2:

$$P_{wind} = \rho U_1 A \cdot \frac{1}{2} \cdot U_1^2 = \frac{1}{2} \rho A U_1^3 \tag{3.67}$$

The power extracted from the wind, $P_{turbine}$ is

$$P_{turbine} = \rho U A \left(\frac{U_1^2}{2} - \frac{U_\infty^2}{2} \right) \tag{3.68}$$

Let us assume

$$U \approx U_1^{-\Delta U_\infty/2}; U_\infty = U_1 - \Delta U_\infty; \Psi = \frac{\Delta U_\infty}{U_1} \tag{3.69}$$

The efficiency limit, η_{ideal}, is as follows:

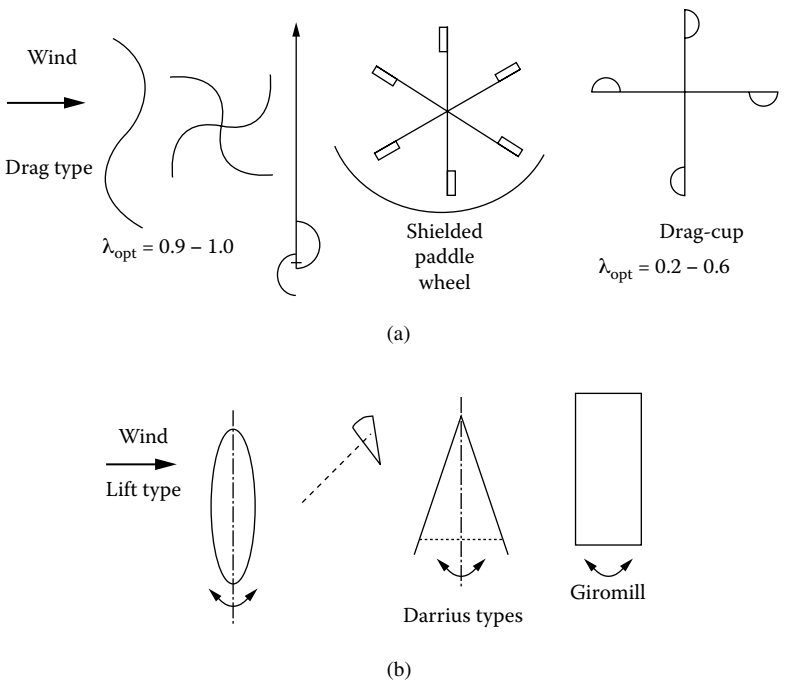

FIGURE 3.52 Tangential (vertical shaft) wind turbines: (a) drag subtype and (b) lift subtype.

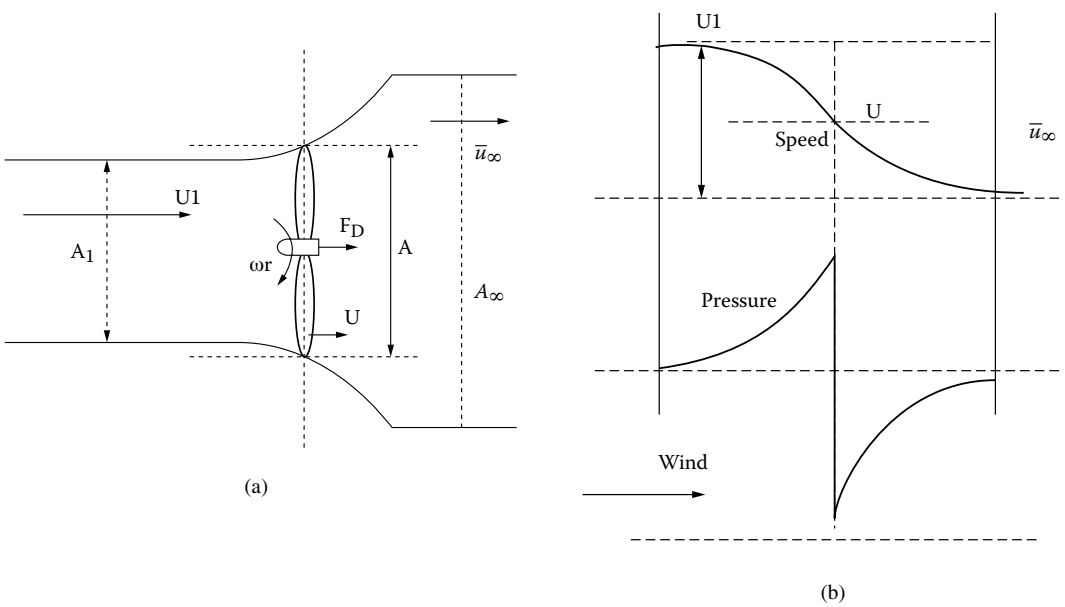

FIGURE 3.53 (a) Basic wind turbine speed and (b) pressure variation.

$$\eta_{ideal} = \frac{P_{turbine}}{P_{wind}} = \frac{\frac{1}{2}\rho UA\left(U_1^2 - U_\infty^2\right)}{\frac{1}{2}\rho A U_1^3} \tag{3.70}$$

With Equation 3.60, η_{ideal} becomes

$$\eta_{ideal} = \left(1 - \frac{\Psi}{2}\right)\left[1 - \left(1 - \Psi\right)^2\right] \tag{3.71}$$

The maximum ideal efficiency is obtained for $\partial\eta_i / \partial\Psi = 0$ at $\Psi_{opt} = 2/3$ ($U_\infty/U_1 = 1/3$) with $\eta_{imax} = 0.593$. This ideal maximum efficiency is known as the Betz limit [26].

3.9.2 The Steady-State Model of Wind Turbines

The steady-state behavior of wind turbines is carried out usually through the blade element momentum (BEM) model. The blade is divided into a number of sections with geometrical, mechanical, and aerodynamic properties that are given as functions of the local radius from the hub. At the local radius, the cross-sectional airfoil element of the blade is shown in Figure 3.54.

The local relative velocity $U_{rel}(r)$ is obtained by superimposing the axial velocity $U(1 - a)$ and the rotation velocity $r\omega_r(1 + a')$ at the rotor plane.

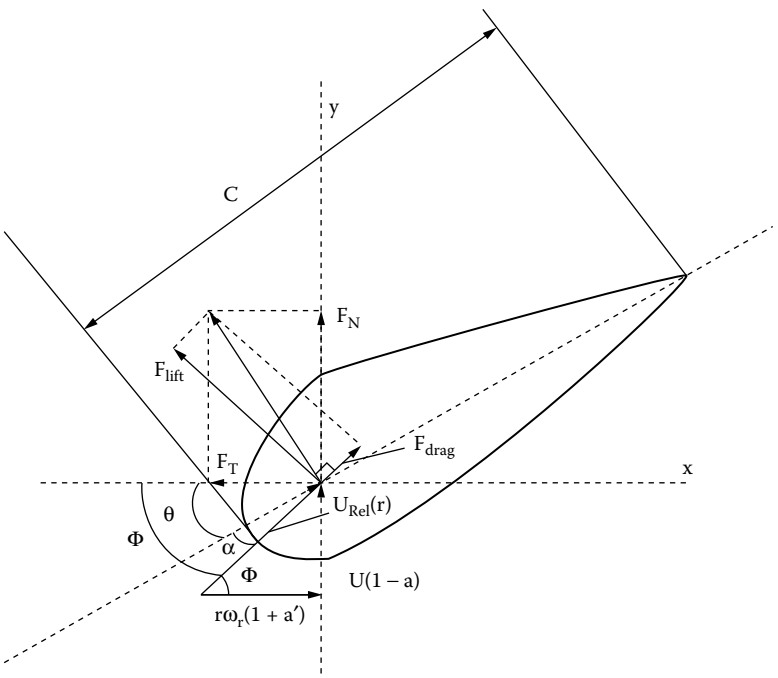

FIGURE 3.54 Blade element with pertinent speed and forces.

The induced velocities ($-aU$ and $a'r\omega_r$) are produced by the vortex system of the machine.

The local attack angle is as follows:

$$\alpha = \phi - \theta \tag{3.72}$$

with

$$\tan\phi = \frac{U\left(1-a\right)}{r\omega_r\left(1+a'\right)} \tag{3.73}$$

The local blade pitch θ is as follows:

$$\theta = \tau + \beta \tag{3.74}$$

with τ the local blade twist angle and β the global pitch angle.

The lift force F_{lift} is rectangular to U_{rel}, while the drag force F_{drag} is parallel to it. The lift and drag forces F_{lift} and F_{drag} may be written as follows:

$$F_{lift} = \frac{1}{2}\rho U_{rel}\cdot C\cdot C_L;\rho = 1.225\ kg/m^3 \tag{3.75}$$

$$F_{drag} = \frac{1}{2}\rho U_{rel}\cdot C\cdot C_D \tag{3.76}$$

C is the local chord of the blade section and C_L and C_D are lift and drag coefficients, known for a given blade section [26, 27].

From lift and drag forces, the normal force thrust, F_N, and tangential force F_T (along X,Y on the blade section plane) are simply as follows:

$$F_N(r) = F_{lift}\cos\Phi + F_{drag}\sin\Phi \tag{3.77}$$

$$F_T(r) = F_{lift}\sin\Phi - F_{drag}\cos\Phi \tag{3.78}$$

Additional corrections are needed to account for the finite number of blades (B), especially for large values of a (axial induction factor).

Now, the total thrust F_N per turbine is

$$F_T = B\int_0^{Dr/2} F_N(r)dr \tag{3.79}$$

Similarly, the mechanical power P_T is

$$P_T = B\cdot\omega_r\cdot\int_0^{Dr/2} rF_T(r)dr \tag{3.80}$$

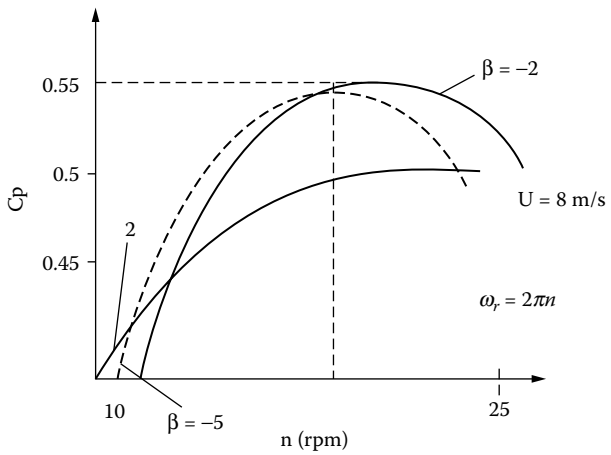

FIGURE 3.55 Typical $C_p - n(\lambda) - \beta$ curves.

Now, with the earlier definition (Equation 3.64), the power efficiency C_p may be calculated. This may be done using a set of airfoil data for the given wind turbine, when a, a', C_L, and C_D are determined first. A family of curves $C_p - \lambda - \beta$ is thus obtained. This, in turn, may be used to investigate the steady-state performance of the wind turbine for various wind speeds U and wind turbine speeds ω_r.

As the influence of blade global pitch angle β is smaller than the influence of tip speed ratio λ in the power efficiency coefficient C_p, we may first keep β = ct. and vary λ for a given turbine. Typical $C_p(\lambda)$ curves are shown in Figure 3.55 for three values of β.

For the time being, let β = ct. and rewrite Equation 3.64 using λ (tip speed ratio):

$$P_M = \frac{1}{2}\rho C_p \pi D_r^2 U^3 = \frac{1}{2}\rho\pi\left(\frac{D_r}{2}\right)^5 \cdot \frac{C_p}{\lambda^3}\omega_r^3 \tag{3.81}$$

Adjusting turbine speed ω_r, that is λ, the optimum value of λ corresponds to the case when C_p is maximum, $C_{p\max}$ (Figure 3.55). Consequently, from Equation 3.81,

$$P_M^{opt} = \frac{1}{2}\rho\pi\left(\frac{D_r}{2}\right)^5 \cdot \frac{C_{p\max}}{\lambda_{opt}^3}\omega_r^3 = K_W\omega_r^3 \tag{3.82}$$

Basically, the optimal turbine power is proportional to the third power of its angular speed (Figure 3.56). Within the optimal power range, the turbine speed ω_r should be proportional to wind speed U as follows:

$$\omega_r = U \cdot \frac{2}{D_r} \cdot \lambda_{opt} \tag{3.83}$$

Above the maximum allowable turbine speed, obtained from mechanical or thermal constraints in the turbine and electric generator, the turbine speed remains constant. As expected, in turbines with constant speed — imposed by the generator to produce constant frequency and voltage power output — the power efficiency constant C_p varies with wind speed (ω_r = ct.) and less-efficient wind energy extraction is performed. Typical turbine power vs. turbine speed curves are shown in Figure 3.57.

Variable-speed operation — which needs power electronics on the generator side — produces considerably more energy only if the wind speed varies considerably in time (inland sites). This is not

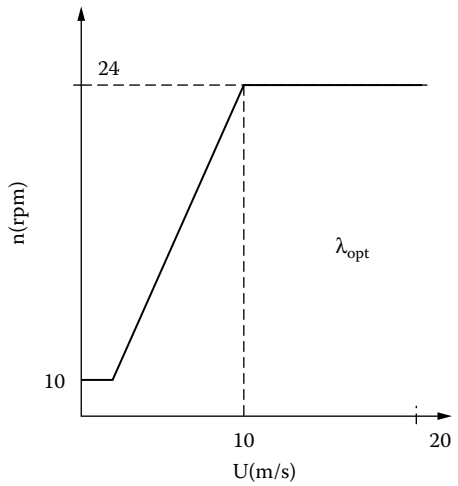

FIGURE 3.56 Typical optimum turbine/wind speed correlation.

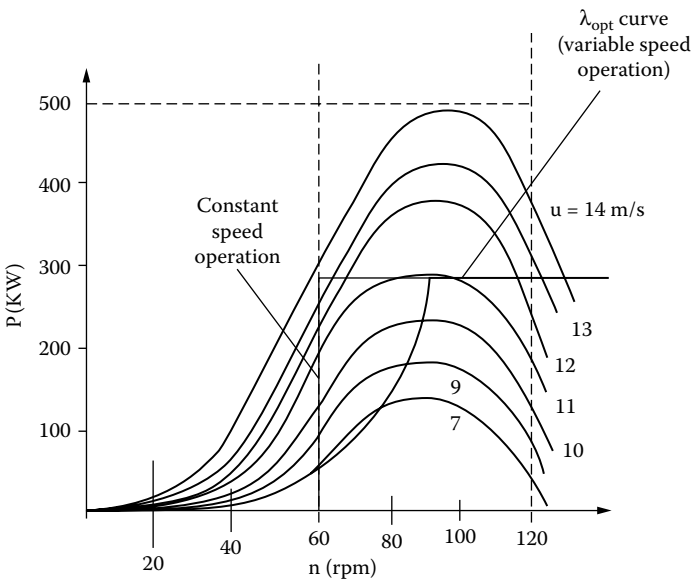

FIGURE 3.57 Turbine power vs. turbine speed for various wind speed u values.

so in on- or offshore sites, where wind speed variations are smaller. However, the flexibility brought by variable speed in terms of electric power control of the generator and its power quality, with a reduction in mechanical stress, in general (especially the thrust and torque reduction), favors variable-speed wind turbines.

There are two methods (Figure 3.58) used to limit power during strong winds ($U > U_{rated}$):

- Stall control
- Pitch control

Stalled blades act as a "wall in the wind." Stall occurs when the angle α between airflow and the blade chord is increased so much that the airflow separates from the airfoil on the suction side to limit the torque-producing force to its rated value. For passive stall, angle β stays constant, as no mechanism to turn the blades is provided. With a mechanism to turn the blades in place above rated wind speed U_{rated},

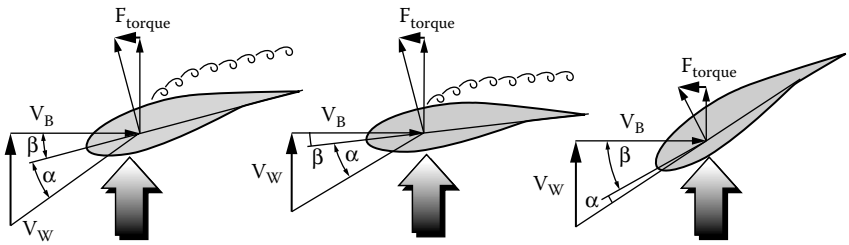

FIGURE 3.58 Stall and pitch control above rated wind speed U_{rated}.

to enforce stall, the angle β is decreased by a small amount. This is the active stall method that may be used at low speeds to increase power extraction by increasing the power efficiency factor C_p (Figure 3.55).

With the pitch control (Figure 3.58), the blades are turned by notably increasing the angle β. The turbine turns to the position of the "flag in the wind" so that aerodynamic forces are reduced. As expected, the servodrive — for pitch control — to change β has to be designed for a higher rating rather than for an active stall.

3.9.3 Wind Turbine Models for Control

Besides slow variations of wind with days or seasons, there are also under 1 Hz and over 1 Hz random wind-speed variations (Figure 3.59) due to turbulence and wind gusts. Axial turbines (with two or three blades) experience two or three speed pulsations per revolution when the blades pass in front of the tower. Tower sideways oscillations also induce shaft speed pulsations. Mechanical transmission and the elasticity of blades, blade fixtures, and couplings produce additional oscillations. The pitch-servo dynamics also has to be considered.

The wind-speed spectrum of a wind turbine located in the wake of a neighboring one in a wind park may also change. Care must be exercised when placing the components of a wind park [29].

Finally, electric load transients or faults produce speed variations.

All of the above clearly indicate intricacy of wind turbine modeling for transients and control.

3.9.3.1 Unsteady Inflow Phenomena in Wind Turbines

The blade element momentum (BEM) model is based in steady state. It presupposes that an instant change of wind profile can take place (Figure 3.59). Transition from state (1) to state (2) in Figure 3.59 corresponds to an increase of global pitch angle β by the pitch-servo.

Experiments have shown that in reality there are at least two time constants that delay the transition: one related to D_r/U and the other related to $2C/(D_r\omega_r)$ [30].

Time lags are related to the axial- and tangential-induced velocities ($-aU$ and $+a'D_r\omega_r/2$).

The inclusion of a lead–lag filter to simulate the inflow phenomena seems insufficient due to considerable uncertainty in the modeling.

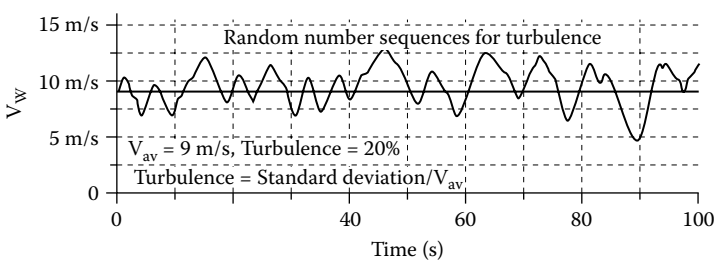

FIGURE 3.59 Typical wind-speed variations with time.

3.9.3.2 The Pitch-Servo and Turbine Model

The pitch-servo is implemented as a mechanical hydraulic or electrohydraulic governor. A first-order (Figure 3.60) or a second-order model could be adopted. In Figure 3.60, the pitch-servo is modeled as a simple delay T_{servo}, while the variation slope is limited between $d\beta_{min}/dt$ and $d\beta_{max}/dt$ (to take care of inflow phenomena). Also, the global attack angle β span is limited from $\beta_{optimum}$ to $\beta_{maximum}$. β_{opt} is obtained from the $C_p - \lambda - \beta$ curve family for C_{pmax} with respect to β (Figure 3.61, [28]).

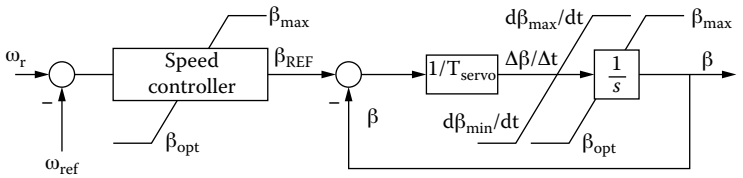

(a)

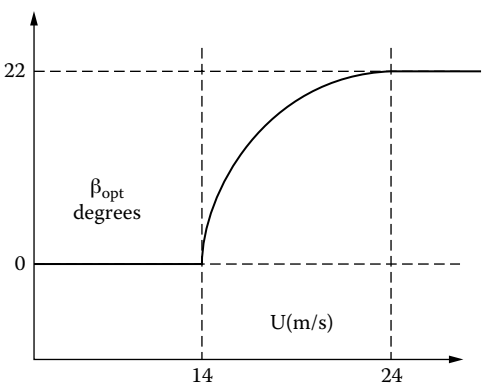

(b)

FIGURE 3.60 Pitch-servo model and (a) control and (b) optimum $\beta(U)$ for variable speed.

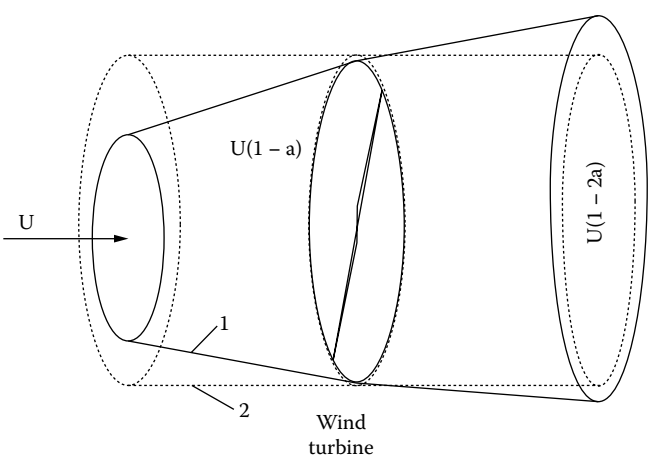

FIGURE 3.61 Wind profile transition from state to state.

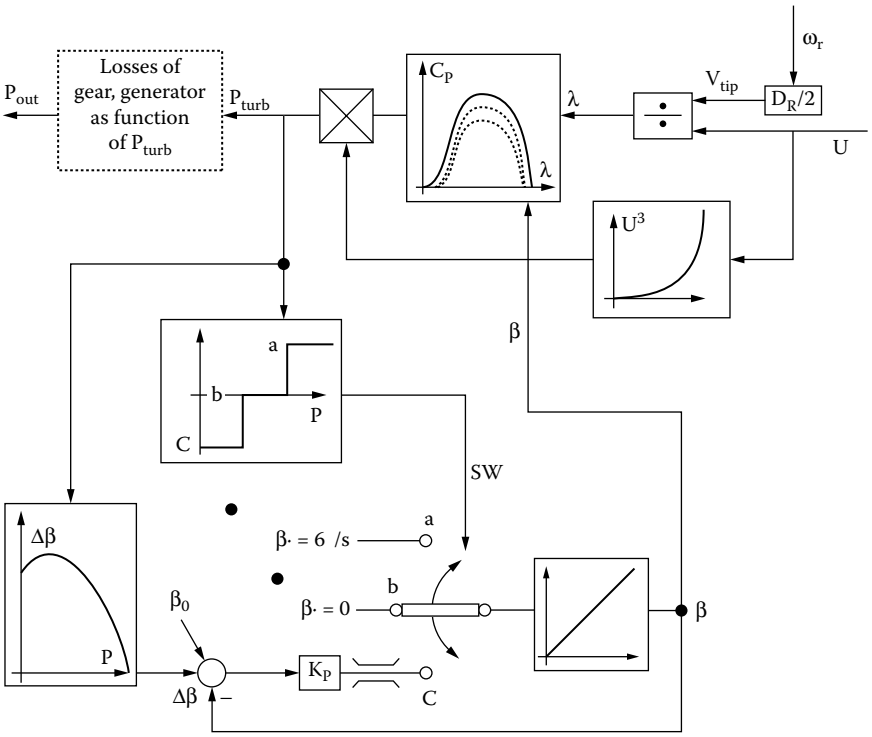

FIGURE 3.62 Simplified structural diagram of the constant speed wind turbine with active stall.

Now, from angle β to output power, the steady-state model of the wind turbine is used (Figure 3.62) for a constant-speed active-stall wind turbine. When the turbine produces more than the rated power, the switch is in position *a*, and the angle β is increased at the rate of 6 /sec to move the blades toward the "flag in the wind" position. When the power is around the rated value, the pitch drive stays idle with $\beta = 0$; thus, β is constant (position b). Below rated power, the switch goes to position "C" and a proportional controller (K_p) produces the desired β. The reference value β^* corresponds to its optimum value as a function of mechanical power, that is, maximum power. This is only a sample of the constant-speed turbine model with pitch-servo control for active stall above rated power and $\beta_{optimization}$ control below rated power.

As can be seen from Figure 3.62, the model is highly nonlinear. Still, because of the delays due to inflow phenomena, the elasticities of various elements of the turbine are not yet included. Also, the model of the pitch-servo is not included. Usually, there is a transmission between the wind turbine and the electric generator. A six-order drive train is shown in Figure 3.63.

Inertias of hub, blades, gearbox, and generator are denoted by H_i. Each part has a spring and a dashpot element. The matrix dynamic equation of the drive train is of the following form [31]:

$$\frac{d}{dt}\begin{bmatrix}|\theta| \\ |\omega|\end{bmatrix} = \begin{bmatrix}0 & I \\ -\left[2H^{-1}\right][C] & -\left[2H^{-1}\right]D\end{bmatrix}\cdot\begin{bmatrix}|\theta| \\ |\omega|\end{bmatrix} + \begin{bmatrix}0 \\ 2H^{-1}\end{bmatrix}[T] \tag{3.84}$$

A few "real-world" pulsations in speed or electric power may be detected by such models; resonance conditions may be avoided through design or control measures.

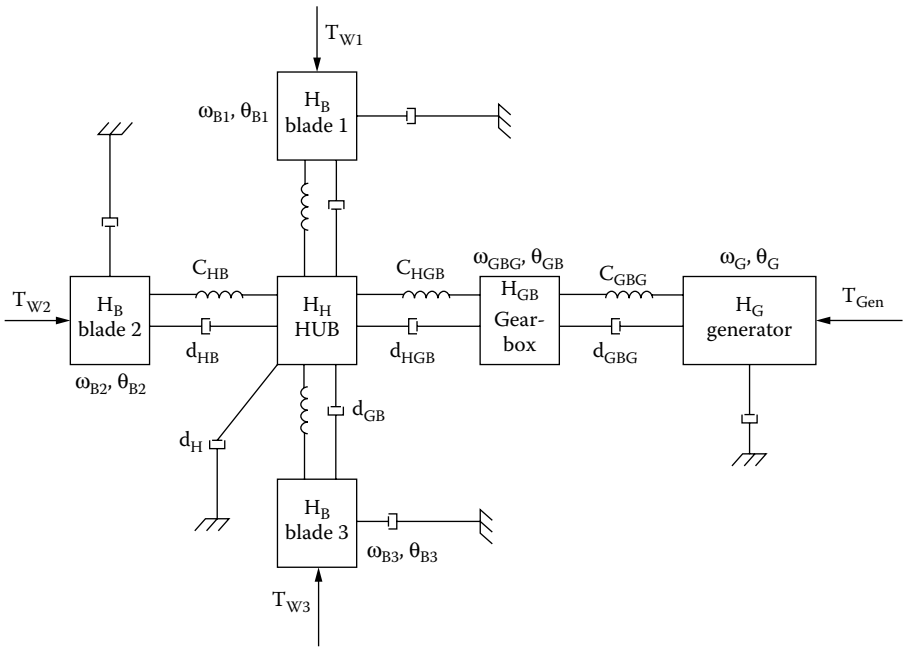

FIGURE 3.63 Six-inertia drive train.

3.10 Summary

- Prime movers are mechanical machines that convert the primary energy of a fuel (or fluid) into mechanical energy.
- Prime movers drive electric generators connected to the power grid or operating in isolation.
- Steam and gas turbines and internal combustion engines (spark-ignited or diesel) are burning fossil fuels to produce mechanical work.
- Steam turbines contain stationary and rotating blades grouped into high-, intermediate-, and low-pressure (HP, IP, LP) sections on the same shaft in tandem-compound and on two shafts in cross-compound configurations.
- Between stages, steam engines use reheaters: single reheat and doubly reheat, at most.
- In steam turbines, typically, the power is divided as follows: 30% in the HP stage, 40% in the IP stage, and 30% in the LP stage.
- Governor valves (GVs) and intercept valves (IVs) are used to control the HP and, respectively, LP stages of the steam flow.
- The steam vessel may be modeled by a first-order delay, while the steam turbine torque is proportional to its steam flow rate.
- Three more delays related to inlet and steam chest, to the reheater, and to the crossover piping may be identified.
- Speed governors for steam turbines include a speed relay with a first-order delay and a hydraulic servomotor characterized by a further delay.
- Gas turbines burn natural gas in combination with air that is compressed in a compressor driven by the gas turbine.
- The 500 C gas exhaust is used to produce steam that drives a steam turbine placed on the same shaft. These combined-cycle unishaft gas turbines are credited with a total efficiency above 55%. Combined-cycle gas turbines at large powers seem to be the way of the future. They are also introduced for cogeneration in high-speed small- and medium-power applications.

- Diesel engines are used from the kilowatt range to the megawatt range power per unit for cogeneration or for standby (emergency) power sets.
- The fuel injection control in diesel engines is performed by a speed governing system.
- The diesel engine model contains a nonconstant gain. The gain depends on the engine equivalence ratio (eer), which, in turn, is governed by the fuel/air ratio; a dead time constant dependent on engine speed is added to complete the diesel engine model.
- Diesel engines are provided with a turbocharger that has a turbine "driven" by the fuel exhaust that drives a compressor, which provides the hot high-pressure air for the air mix of the main engine. The turbocharger runs freely at high speed but is coupled to the engine at low speed.
- Stirling engines are "old" thermal piston engines with continuous heat supply. Their thermal cycles contain two isotherms. In a basic configuration, the engine consists of two opposed pistons and a regenerator in between. The efficiency of the Stirling engine is temperature limited.
- Stirling engines are independent fuel types; they use air, methane, He, or H_2 as working fluids. They did not reach commercial success as a kinetic type due to problems with the regenerator and stabilization.
- Stirling engines with free piston-displacer mover and linear motion recently reached the market in units in the 50 W to a few kilowatts.
- The main merits of Stirling engines are related to their quietness and reduced noxious emissions, but they tend to be expensive and difficult to stabilize.
- Hydraulic turbines convert the water energy of rivers into mechanical work. They are the oldest prime movers.
- Hydraulic turbines are of the impulse type for heads above 300 to 400 m and of reaction type for heads below 300 m. In a more detailed classification, they are tangential (Pelton), radial–axial (Francis), and axial (Kaplan, Bulb, Straflo).
- High head (impulse) turbines use a nozzle with a needle controller, where water is accelerated, and then it impacts the bowl-shaped buckets on the water wheel of the turbine. A jet deflector deflects water from the runner to limit turbine speed when the electric load decreases.
- Reaction turbines — at medium and low head — use wicket gates and rotor blade servomotors to control water flow in the turbine.
- Hydraulic turbines may be modeled by a first-order model if water hammer (wave) and surge effects are neglected. Such a rough approximation does not hold above 0.1 Hz.
- Second-order models for hydraulic turbines with water hammer effect in the penstock are considered valid up to 1 Hz. Higher orders are required above 1 Hz, as the nonlinear model has a gain with amplitude that varies periodically. Second- or third-order models may be identified from tests through adequate curve-fitting methods.
- Hydraulic turbine governors have one or two power levels. The lower power level may be electric, while the larger (upper) power level is a hydraulic servomotor. The speed controller of the governor traditionally has a permanent drop and a transient drop.
- Modern nonlinear control systems may now be used to simultaneously control the guide vane runner and the blade runner.
- Reversible hydraulic machines are used for pump-storage power plants or for tidal-wave power plants. The optimal pumping speed is about 12 to 20% above the optimal turbining speed. Variable-speed operation is required. So, power electronics on the electric side are mandatory.
- Wind turbines use the wind air energy. Nonuniformity and strength vary with location height and terrain irregularities. Wind speed duration vs. speed, speed vs. frequency, and mean (average) speed using Raleigh or Weibull distribution are used to characterize wind at a location in time. The wind-turbine-rated wind speed is generally 150% of mean wind speed.
- Wind turbines can be found in two main types: axial (with horizontal shaft) and tangential (with vertical shaft).

- The main steady-state parameter of wind turbines is the power efficiency coefficient C_p, which is dependent upon blade tip speed $R\omega_r$ to wind speed U (ratio λ). C_p depends on λ and on blade absolute attack angle β.
- The maximum C_p (0.3 to 0.4) is obtained for $\lambda_{opt} \leq 1$ for low-speed axial turbines and $\lambda_{opt} \geq 1$ for high-speed turbines.
- The ideal maximum efficiency limit of wind turbines is about 0.6 (Betz limit).
- Wind impacts on the turbine a thrust force and a torque. Only torque is useful. The thrust force and C_p depend on blade absolute attack angle β.
- The optimal power $P_T(\lambda_{opt})$ is proportional to u^3 (u is the wind speed).
- Variable-speed turbines will collect notably more power from a location if the speed varies significantly with time and season, such that λ may be kept optimum. Above the rated wind speed (and power), the power is limited by passive-stall, active-stall, or pitch-servo control.
- Wind turbine steady-state models are highly nonlinear. Unsteady inflow phenomena show up in fast transients and have to be accounted for by more than lead–lag elements.
- Pitch-servo control is becoming more frequently used, even with variable-speed operation, to allow speed limitation during load transients or power grid faults.
- First- or second-order models may be adopted for speed governors. Elastic transmission multimass models have to be added to complete the controlled wind turbine models for transients and control [32].
- Prime-mover models will be used in the following chapters, where electric generator control will be treated in detail.

References

1. R. Decker, *Energy Conversion*, Oxford University Press, Oxford, 1994.
2. P. Kundur, *Power System Stability and Control*, McGraw-Hill, New York, 1994.
3. J. Machowski, J.W. Bialek, and J.R. Bumby, Power System Dynamics and Stability, John Wiley & Sons, New York, 1997.
4. IEEE Working Group Report, Steam models for fossil fueled steam units in power-system studies, *IEEE Trans.*, PWRS-6, 2, 1991, pp. 753–761.
5. S. Yokokawa, Y. Ueki, H. Tanaka, Hi Doi, K. Ueda, and N. Taniguchi, Multivariable adaptive control for a thermal generator, *IEEE Trans.*, EC-3, 3, 1988, pp. 479–486.
6. G.K. Venayagomoorthy, and R.G. Harley, A continually on line trained microcontroller for excitation and turbine control of a turbogenerator, *IEEE Trans.*, EC-16, 3, 2001, pp. 261–269.
7. C.F. Taylor, *The Internal-Combustion Engine in Theory and Practice, vol. II: Combustion, Fuels, Materials, Design*, The MIT Press, Cambridge, MA, 1968.
8. P.M. Anderson, and M. Mirheydar, Analysis of a diesel-engine driven generating unit and the possibility for voltage flicker, *IEEE Trans.*, EC-10, 1, 1995, pp. 37–47.
9. N. Watson, and M.S. Janota, *Turbocharging the Internal Combustion Engine*, Macmillan, New York, 1982.
10. S. Roy, O.P. Malik, and G.S. Hope, Adaptive control of speed and equivalence ratio dynamics of a diesel driven power plant, *IEEE Trans.*, EC-8, 1, 1993, pp. 13–19.
11. A. Kusko, *Emergency Stand-by Power Systems*, McGraw-Hill, New York, 1989.
12. K.E. Yoager, and J.R. Willis, Modelling of emergency diesel generators in an 800 MW nuclear power plant, *IEEE Trans.*, EC-8, 3, 1993, pp. 433–441.
13. U. Kieneke, and L. Nielsen, *Automotive Control Systems*, Springer-Verlag, Heidelberg, 2000.
14. G. Walker, O.R. Fauvel, G. Reader, and E.R. Birgham, *The Stirling Alternative*, Gordon and Breach Science Publishers, London, 1994.
15. R.W. Redlich, and D.W. Berchowitz, Linear dynamics of free piston Stirling engine, *Proc. of Inst. Mech. Eng.*, March 1985, pp. 203–213.

16. M. Barglazan, *Hydraulic Turbines and Hydrodynamic Transmissions*, University Politechnica of Timisoara, Romania, 1999.
17. IEEE Working Group on Prime Mover and Energy Supply, Hydraulic turbine and turbine control models for system stability studies, *IEEE Trans.*, PS-7, 1, 1992, pp. 167–179.
18. C.D. Vournas, Second order hydraulic turbine models for multimachine stability studies, *IEEE Trans.*, EC-5, 2, 1990, pp. 239–244.
19. C.K. Sanathanan, Accurate low order model for hydraulic turbine-penstock, *IEEE Trans.*, EC-2, 2, 1987, pp. 196–200.
20. D.D. Konidaris, and N.A. Tegopoulos, Investigation of oscillatory problems of hydraulic generating units equipped with Francis turbines, *IEEE Trans.*, EC-12, 4, 1997, pp. 419–425.
21. D.J. Trudnowski, and J.C. Agee, Identifying a hydraulic turbine model from measured field data, *IEEE Trans.*, EC-10, 4, 1995, pp. 768–773.
22. J.E. Landsberry, and L. Wozniak, Adaptive hydrogenerator governor tuning with a genetic algorithm, *IEEE Trans.*, EC-9, 1, 1994, pp. 179–185.
23. Y. Zhang, O.P. Malik, G.S. Hope, and G.P. Chen, Application of inverse input/output mapped ANN as a power system stabilizer, *IEEE Trans.*, EC-9, 3, 1994, pp. 433–441.
24. M. Djukanovic, M. Novicevic, D. Dobrijovic, B. Babic, D.J. Sobajic, and Y.H. Pao, Neural-net based coordinated stabilizing control of the exciter and governor loops of low head hydropower plants, *IEEE Trans.*, EC-10, 4, 1995, pp. 760–767.
25. T. Kuwabara, A. Shibuya, M. Furuta, E. Kita, and K. Mitsuhashi, Design and dynamics response characteristics of 400 MW adjustable speed pump storage unit for Obkawachi power station, *IEEE Trans.*, EC-11, 2, 1996, pp. 376–384.
26. L.L. Freris, *Wind Energy Conversion Systems*, Prentice Hall, New York, 1998.
27. V.H. Riziotis, P.K. Chaviaropoulos, and S.G. Voutsinas, Development of the State of the Art Aerolastic Simulator for Horizontal Axis Wind Turbines, Part 2: Aerodynamic Aspects and Application, *Wind Eng.*, 20, 6, 1996, pp. 223–440.
28. V. Akhmatov, Modelling of Variable Speed Turbines with Doubly-Fed Induction Generators in Short-Term Stability Investigations, paper presented at the Third International Workshop on Transmission Networks for Off-Shore Wind Farms, Stockholm, Sweden, April 11–12, 2002.
29. T. Thiringer, and J.A. Dahlberg, Periodic pulsations from a three-bladed wind turbine, *IEEE Trans.*, EC-16, 2, 2001, pp. 128–133.
30. H. Suel, and J.G. Schepers, Engineering models for dynamic inflow phenomena, *J. Wind Eng. Ind. Aerodynamics*, 39, 2, 1992, pp. 267–281.
31. S.A. Papathanassiou, and M.P. Papadopoulos, Mechanical stress in fixed-speed wind turbines due to network disturbances, *IEEE Trans.*, EC-16, 4, 2001, pp. 361–367.
32. S.H. Jangamshatti, and V.G. Rau, Normalized power curves as a tool for identification of optimum wind turbine generator parameters, *IEEE Trans.*, EC-16, 3, 2001, pp. 283–288.